ELSEVIER

J. Non-Newtonian Fluid Mech. 110 (2003) 143–176

Journal of Non-Newtonian Fluid Mechanics

www.elsevier.com/locate/jnnfm

Vortex shedding in cylinder flow of shear-thinning fluids I. Identification and demarcation of flow regimes

P.M. Coelho, F.T. Pinho*

Centro de Estudos de Fenómenos de Transporte, DEMEGI, Faculdade de Engenharia da Universidade do Porto, Rua Dr. Roberto Frias S/N 4200-465, Porto, Portugal

Received 29 July 2002; received in revised form 3 January 2003

Abstract

An experimental study on the flow of non-Newtonian fluids around a cylinder was undertaken to identify and delimit the various shedding flow regimes as a function of adequate non-dimensional numbers. The measurements of vortex shedding frequency and formation length (l_f) were carried out by laser-Doppler anemometry in Newtonian fluids and in aqueous polymer solutions of CMC and tylose. These were shear thinning and elastic at weight concentrations ranging from 0.1 to 0.6%. The 10 and 20 mm diameter cylinders (D) used in the experiments had aspect ratios of 12 and 6 and blockage ratios of 5 and 10%, respectively. The Reynolds number (Re^*) was based on a characteristic shear rate of $U_\infty/(2D)$ and ranged from 50 to 9×10^3 thus encompassing the laminar shedding, the transition and shear-layer transition regimes. Increasing fluid elasticity reduced the various critical Reynolds numbers (Re^*_{etr}, Re^*_{lf}, Re^*_{bbp}) and narrowed the extent of the transition regime. For the 0.6% tylose solution the transition regime was even suppressed. On the other end, pseudoplasticity was found to be indirectly responsible for the observed reduction in Re^*_{otr}: it increases the Strouhal number which in turn increases the vortex filaments, precursors of the transition regime. Elasticity was better quantified by the elasticity number Re'/We than by the Weissenberg number. This elasticity number involves the calculation of the viscosity at a high characteristic shear rate, typical of the boundary layer, rather than at the average value ($U_\infty/(2D)$) used for the Reynolds number, Re^*.

Keywords: Cylinder flow; Viscoelastic; Shear thinning; Dilute polymeric solutions; Relaxation time; Vortex shedding; Strouhal number; Laminar; Transition

1. Introduction

Studies of the flow around a cylinder are fundamental to a comprehensive understanding of more complex flows around bluff bodies or rod bundles, the latter of particular relevance in tube-shell heat exchangers. Many engineering processes of the food, detergent and other chemical and processing

* Corresponding author. Tel.: +351-225-081-762; fax: +351-225-081-763/445.
E-mail address: fpinho@fe.up.pt (F.T. Pinho).

0377-0257/03/$ – see front matter © 2003 Elsevier Science B.V. All rights reserved.
doi:10.1016/S0377-0257(03)00007-7

Nomenclature

D	cylinder diameter (m)
f	vortex shedding frequency (s^{-1})
k	consistency index (Pa s^n)
l_d	diffusion length (m)
l_f	formation length (m)
L	cylinder length (m)
n	power-law index
N	number of measurements of streamwise normal Reynolds stress, taken along the near-wake symmetry plane
r	radial co-ordinate measured from the center of the cylinder (m)
R	cylinder radius (m)
Re	Reynolds number ($Re \equiv \rho U_\infty D/\eta_{ch}$)
ΔRe	extent of the transition regime (Re_{etr}–Re_{otr})
s	arc length from the forward stagnation point ($s = \phi R$)
St	Strouhal number ($St \equiv fD/U_\infty$)
u	local streamwise velocity (m/s)
u'	streamwise velocity fluctuation (m/s)
$\overline{u'}$	averaged streamwise turbulence in the near-wake symmetry plane, $\overline{u'} \equiv \sum_{i=1}^{N} (\sqrt{\overline{u'^2}})_i / N$ (m/s)
U_∞	free-stream velocity (m/s)
We	Weissenberg number ($We \equiv \lambda_e U_\infty / D$)

Greek letters

$\dot{\gamma}$	shear rate (s^{-1})
γ_0, $\dot{y}_\infty$	intercept and slope of the linear regression applied to the deformation versus time data of the creep test (<, s_{-1})
δ	boundary layer thickness, measured from the cylinder wall up to the radial location, where $\partial u/\partial r = 0$ (m)
η	dynamic viscosity (Pa s)
λ_e	relaxation time (s)
ρ	fluid density (kg/m^3)
ϕ	angular co-ordinate measured from the forward stagnation point

Subscripts

0	zero shear rate
75	75° from forward stagnation point
bbp	end of the region where the power spectra distribution shows a broad basis at peak frequency
ch	characteristic parameter
etr	the end of transition regime
lf	sudden drop in formation length

otr	onset of transition regime
vs	onset of laminar vortex shedding regime
w	wall

Superscripts

#	Reynolds number with η_{ch} at $\dot{\gamma}_{ch} \equiv U_\infty/R$
$'$	Reynolds number with η_{ch} at $\dot{\gamma}_{ch} \equiv \dot{\gamma}_{w,75^\circ}$
$''$	Reynolds number with η_{ch} equal to the average value of viscosity between $\dot{\gamma} = 0$ and $\dot{\gamma} = \dot{\gamma}_{w,75^\circ}$
0	Reynolds number with η_{ch} at $\dot{\gamma}_{ch} \equiv 0$
$*$	Reynolds number with η_{ch} at $\dot{\gamma}_{ch} \equiv U_\infty/(2D)$

Symbology in figures

×	water
+	glycerin and water mixture
●	0.4% CMC
▲	0.3% CMC
◆	0.2% CMC
■	0.1% CMC
○	0.6% tylose
△	0.4% tylose
◇	0.3% tylose
□	0.2% tylose

industries involve heat and mass transfer with non-Newtonian fluids of low viscosity, but the literature on cylinder flows with these fluids is scarce. This is the motivation for this work, which starts by investigating some hydrodynamic characteristics of the cross-flow of shear thinning weakly elastic fluids around a cylinder.

Cylinder flows of Newtonian fluids have been studied for more than 100 years and important seminal works were the early contributions of Strouhal [1], Hiemenz [2] and von Kármán [3], amongst others. These Newtonian flows are relevant in industrial situations similar to those cited above as well as in hydraulics and aeroacustics to name just a few. Since then, there has been a wealth of data and contributions aimed at investigating different aspects of this complex behaviour and some more recent important reviews are by Cantwell and Coles [4], Telionis et al. [5] and Williamson [6].

Knowledge of fundamental cylinder flow characteristics for Newtonian fluids is important to understand the new results presented in this paper for non-Newtonian fluids, therefore we review the relevant Newtonian flow characteristics in Section 2. Much of this work will concentrate on the vortex shedding phenomenon; in this context, it is important to refer the work of Gerrard [7], who proposed a mechanism to explain vortex shedding based on the so-called formation and diffusion lengths. Bloor [8] delimited the formation region (l_f) by the cylinder rear stagnation point and the location where fluid from outside the wake first crosses the symmetry plane, as it is entrained by the opposite shear layer. This entrainment results in a local peak of velocity fluctuations at the end of the formation region. The second characteristic

length, which Gerrard termed the diffusion length (l_d), is the thickness of the free shear layer measured at the end of the formation region. In the mechanism proposed by Gerrard [7] the Strouhal number varies inversely with both l_f and l_d.

Cylinder flows have been far less investigated with non-Newtonian fluids, with most of the contributions being theoretical or numerical, and aimed at the creeping flow regime [9,10]. Shah et al. [11] were among the first to experimentally investigate cross-flows of non-Newtonian fluids around cylinders, up to Reynolds numbers of about 12,000. With shear thinning, elastic, aqueous solutions of CMC, variation of pressure along the cylinder laminar boundary layer was independent of the consistency (k) and power-law (n) indices. The boundary layer theory was extended to predict local heat transfer coefficients of non-Newtonian flows within the $\pm 60^\circ$ cylinder forward region and their experimental results showed significant deviations from Newtonian behaviour.

The measurements of hydrodynamic and heat transfer characteristics of elastic fluids with constant viscosity (nowadays called Boger fluids) by James and Acosta [12] and James and Gupta [13] were limited to lower maximum Reynolds numbers of 50 and 200, respectively. Above a critical Reynolds number, the drag coefficient and Nusselt number were found to be dependent only on the Weissenberg number.

A fairly detailed investigation with constant viscosity fluids was carried out by Sarpkaya et al. [14], who measured the surface pressure distribution, drag force, vortex shedding, angle of separation and some effects of free stream turbulence. They investigated extensively the effects of polymer degradation on the onset of various flow regimes, the laminar-turbulent flow transition and wake hydrodynamics. The presence of additives was found to advance flow characteristics normally observed at higher Reynolds numbers. Their Reynolds number were rather restricted ($5 \times 10^4 < Re < 3 \times 10^5$), but much higher than that in previous works.

Vortex shedding on cylinder flows at a constant Reynolds number of 240 was also studied by Gadd [15] with very dilute solutions of polyethylene oxide (PEO). Using a 0.15 mm diameter cylinder, Gadd also tried to correlate the behaviours of several polymer solutions in cylinder flow with their observed drag reductions in turbulent pipe flow. Although the shedding frequency decreased with the concentration of PEO, it did not change with other polymer additives (guar gum and polyacrylamide), even though all fluids produced the same amount of drag reduction in turbulent pipe flow. For the drag coefficient in sphere flow, White [16] reported similar findings. Kalashnikov and Kuding [17] extended Gadd's work up to a Reynolds number of 400 and investigated the effect of cylinder diameter. Smaller diameters were found to enhance the reduction of shedding frequency, with fluid degradation suppressing these effects at a faster rate than the suppression of drag reduction in turbulent pipe flow. The authors attributed the reduction of shedding frequency to viscoelasticity and, for inelastic fluids they found a higher frequency than for the pure solvent.

Flows of aqueous solutions of polyethylene oxide were again investigated by Usui et al. [18] in the range $40 < Re < 200$, but with larger cylinder diameters. Now, the decrease in Strouhal number was correlated with the Weissenberg number and with the normalised wave propagation velocity given by $\sqrt{Re/We}$.

More recently, Cadot and Kumar [19] observed a decrease in shedding frequency, an increase in the formation length and the inhibition of large-scale structures, that they attributed to fluid elasticity. However, it is important to notice two differences relative to the present work: (1) their fluids were weakly shear thinning (power-law index $n = 0.902$), whereas here n varies from 0.543 up to 0.880; and (2) Cadot and Kumar investigated heterogeneous solutions (the approach flow was Newtonian and concentrated

polymer solutions were injected at the cylinder wall) whereas here, and in the other cited papers, the fluids are homogenous.

Other recent experimental investigations on non-Newtonian cylinder flow were by Bergins et al. [20] and Cressman et al. [21]. In the former work, cationic surfactant solutions were used and suppression of vortex shedding with Reynolds number was found because of the presence of shear-induced structures and its elastic rheology. In the latter work, Cressman et al. investigated a pure two-dimensional flow of polyethylene oxide around a 2 mm cylinder. The solution contained a surfactant to stabilize the "soap" film and, a decrease in vortex shedding frequency, an increase in formation length and the suppression of the rms of the velocity fluctuations were observed.

Numerical investigations on viscoelastic vortex shedding are scarce, as shown by Oliveira [22], who developed an appropriated second-order time descretization scheme to remove artificial diffusion. His predictions with the constant viscosity FENE-CR fluid showed an increase in formation length and a decrease in Strouhal number due to fluid elasticity for Reynolds numbers between 50 and 140. The characteristic Reynolds number marking the onset of periodic vortex shedding was only slightly increased from the Newtonian value of 47–50.

These papers, which represent most of the published work on vortex shedding with polymer solutions, did not assess the effect of shear thinning upon shedding frequency. Besides, their range of Reynolds numbers was usually rather restricted and the influence of polymer concentration on the various regimes of vortex shedding was not an addressed issue.

In this work, we present and discuss new results of measurements of the vortex shedding activity in the wake of cylinders for various aqueous polymer solutions and two Newtonian fluids. The Reynolds numbers encompass the laminar vortex shedding regime, the transition regime and the shear-layer transition regime, and the approach flow is characterised by non-negligible free-stream turbulence.

The next section briefly reviews the main characteristics of cylinder flows with Newtonian fluids which will be helpful to understand the present results. Section 3 describes the rig, the instrumentation and presents the corresponding uncertainties. This is followed in Section 4 by the rheological characterisation of the fluids. The results are then presented and discussed in Section 5, and the paper ends with a summary of the main conclusions.

2. Background: some characteristics of Newtonian cylinder flow

In this work, the Reynolds numbers vary from about 200 to 40,000 for Newtonian fluids, but for non-Newtonian fluids they will be smaller because of their higher viscosities. Nevertheless, the Reynolds numbers still encompass the regimes of laminar vortex shedding, transition and shear-layer transition. In the next few paragraphs, the main characteristics of these flow regimes are briefly summarised for Newtonian fluids. Since the understanding of the effect of end conditions is still incomplete, this description pertains to large cylinder aspect ratios, L/D.

Laminar vortex shedding starts at $Re \approx 47$ and goes up to $Re \approx 150$–200. The characteristic two-dimensional parallel shedding of this flow regime requires closely controlled end conditions. Otherwise, there will be oblique shedding with the vortices emanating from the cylinder at an angle θ relative to its axis, as is very often the case [23,24]. Changes in the shedding angle lead to discontinuities in the Strouhal number (St) variation, but Williamson [25] collapsed the normalised frequency data for oblique (St_θ) and parallel (St_0) shedding by using the transformation $St_0 = St_\theta/\cos\theta$.

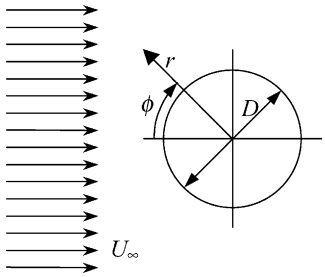

Fig. 1. Cylinder notation and the approach flow.

From the end of the laminar shedding regime up to $Re \approx 260$–400 laminar and turbulent vortices coexist in the spanwise direction [26], defining the so-called transition regime. The wide ranges of limiting Reynolds numbers are due to varying effects of the end condition [27].

The transition regime is subdivided into various sub-regimes [23,27,28], which correspond to discontinuities in the Strouhal number and base-pressure coefficient curves. The base-pressure coefficient C_{pb} is defined as $C_{pb} \equiv (p_b - p_\infty)/(\rho U_\infty^2/2)$, where p_b is the pressure at the base of the cylinder ($\phi = 180^\circ$; Fig. 1), and p_∞ and U_∞ stand for the free-stream static pressure and velocity, respectively. The analysis of the measurements of pressure is left to a future report.

The first discontinuity of the Strouhal number is shown in Fig. 2 and marks the onset of the transition regime in the so-called A-mode at $Re \approx 189$. It results from periodic distortions of the von Kármán vortices leading to streamwise vortices as depicted schematically in Fig. 3 taken from [23]. For $Re > 194$ the Strouhal number suddenly decreases due to the appearance of dislocations (superscript $(*)$) and the shedding mode is now called A* (Fig. 2). This is accompanied by a sudden increase in formation length and enhanced velocity fluctuations in the wake of the cylinder; this transition between sub-regimes has

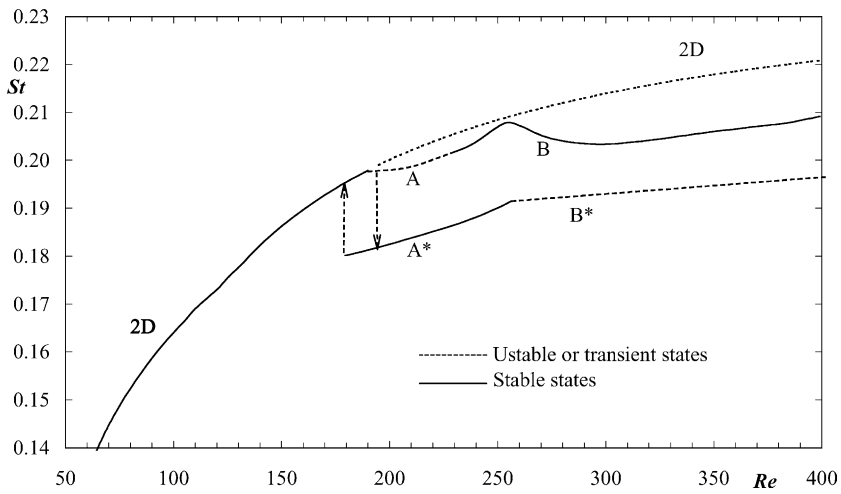

Fig. 2. Qualitative plot showing the Strouhal number variation in the laminar and transition regimes. The upper curve corresponds to small-scale instabilities (A and B) whereas the lower curve corresponds to the coexistence of the same instabilities plus vortex dislocations (from Williamson [6]).

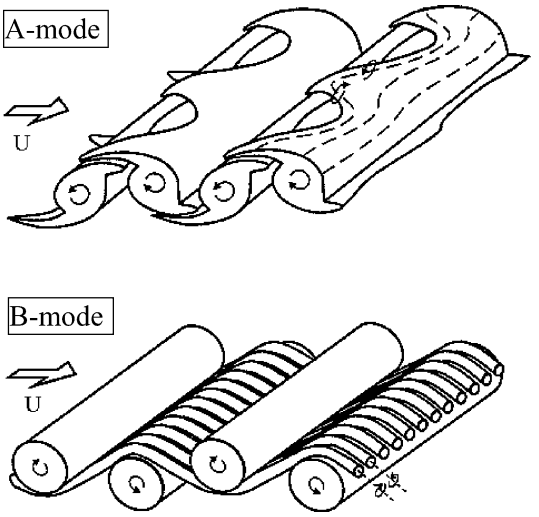

Fig. 3. Schematic representation of primary and secondary vortices in the wake of a cylinder in modes A and B of the shedding mechanism of the transition regime (from Brede et al. [23]).

hysteresis [27]. Further increases in Reynolds number (to about 230–260) sees yet another sudden change in Strouhal number to B-mode (see Fig. 3), but there are also periods of intermittency between modes B* and B.

According to [23], and we cite, "... for the B-mode the vorticity pattern shows spanwise periodicity. Yet, in contrast to the A-mode, the sense of rotation does not change with time for a given spanwise location. Furthermore, the secondary vortices of the B-mode seem to be persistent in time and remain connected over many Kármán cycles. The entire pattern of secondary vortices oscillates up and down sinusoidally during each cycle of Kármán vortex formation." In conclusion, the B-mode is more stable than the A-mode.

For higher Reynolds numbers of up to 1000, the three-dimensional structures in the wake become increasingly disordered and their scales finer. Simultaneously, the Reynolds shear stresses and the base suction coefficient ($-C_{pb}$) decrease and the formation length increases [29].

For *Re* between 1000 and 200,000 transition takes place in the shear-layer as a consequence of the growth of Kelvin–Helmholz instabilities that appear at $350 < Re < 3000$: this scatter in the Reynolds number was attributed, by Prasad and Williamson [30], to the effects of three-dimensional events taking place in the near wake upon the shear-layer flow. In this flow regime, the turbulent shear stress and the suction coefficient increase rapidly, l_f decreases and the transition point moves upstream.

3. Experimental facility

3.1. Water tunnel

The measurements were carried out in the water tunnel shown schematically in Fig. 4, which had a 6:1 contraction (2) before a transparent test section (3) of 197 mm height and 120 mm width. Two

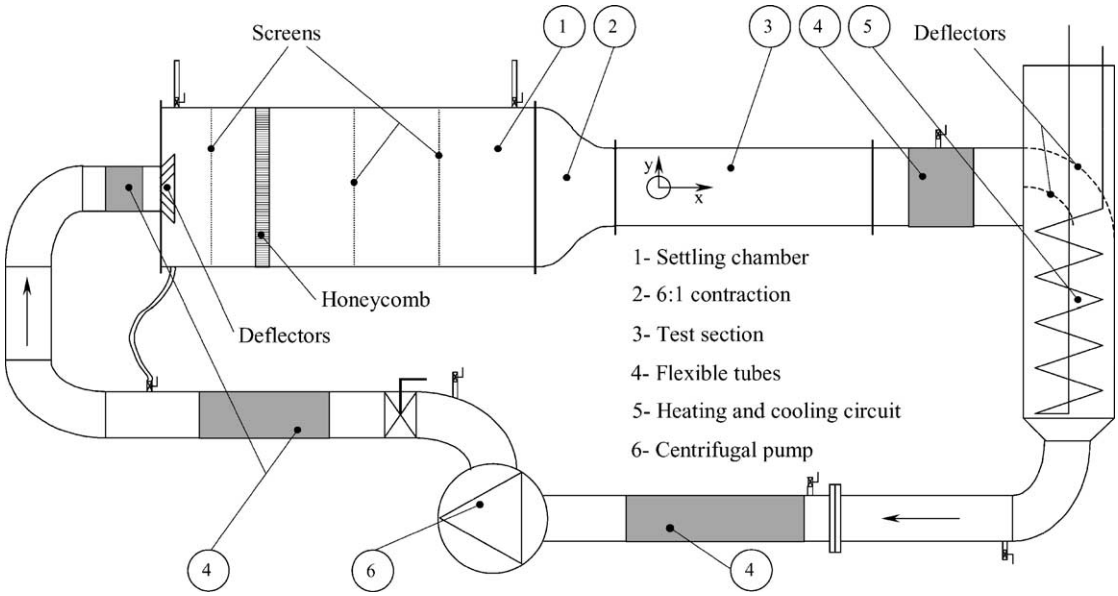

Fig. 4. Schematic representation of the water tunnel.

cylinders were used in the experiments: one had a diameter of 19.7 mm, leading to a blockage of 10% and an aspect ratio of 6:1, and the other had a diameter of 10 mm corresponding to a 5% blockage and a 12:1 aspect ratio. The two cylinders could be mounted at the same place which corresponds to a location 7.5 and 15 cylinder diameters downstream of the test section entrance, respectively. In order to eliminate vibrations, the test section and the settling chamber (1) were isolated from the rest of the rig by means of flexible rubber ducts (4). The maximum mean velocity in the test section was about 2 m/s for all fluids, corresponding to a maximum flowrate of 173 m^3/h. At the inlet of the test section, but outside the wall boundary layers, the mean velocity profile was constant to within 1% and the mean free-stream turbulence was lower than 10% for the viscous Newtonian and all non-Newtonian fluids.

For the water flows the free-stream turbulence is higher, reaching 60% at the lowest Reynolds number, as can be seen in Fig. 5. These results with water are only used in comparisons with data from the Newtonian literature. For the comparisons with the non-Newtonian data only the data from the lower free-stream turbulence glycerine–water flows are used.

The levels of free-stream turbulence in the various flows is a consequence of an abrupt entrance in a too short settling chamber.

The fluid rheology was measured periodically during the experiments to assess its degradation by mechanical scission of the molecules. The fluids were substituted frequently (every 6–20 h depending on the fluid resistance) to limit changes in fluid properties to no more than 10% relatively to those of the fresh solution. The volume of the rig was 450 l and with these large amounts of fluid there were no problems of reproducibility in rheological properties of the solutions, even with daily variations in tap water [31].

A heat exchanger (5) helped maintain the temperature of the working fluid at $25 \pm 0.5\,^{\circ}$C.

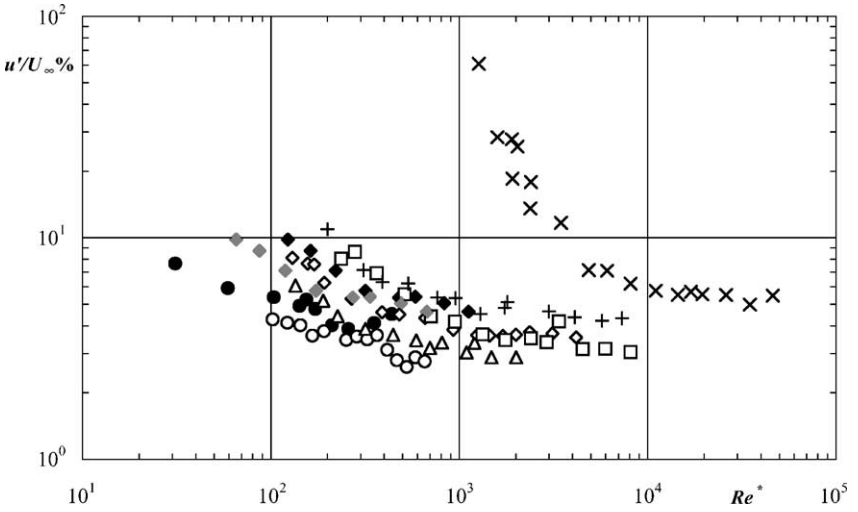

Fig. 5. Variation of streamwise free-stream turbulence with the Reynolds number for various Newtonian and non-Newtonian solutions (black symbols: 20 mm cylinder; grey symbols: 10 mm cylinder). Symbols as in symbology.

3.2. Blockage and end effects

Blockage of the cross-section by the model increases the flow velocity, but does not affect the Strouhal number and has a negligible influence upon the pressure distribution, provided the blockage ratio does not exceed 6% [32]. The minimisation of this effect requires the use of large test sections, and/or smaller diameter cylinders. In the present case, further reduction in cylinder diameter would deteriorate the accuracy of the laser-Doppler anemometry measurements, whereas an increased test section would require larger volumes of liquid and this would also be impractical. As an alternative, corrections could be used, but none of the presently available methods is widely accepted [33,34] and even less so for non-Newtonian fluids. West and Apelt [32] showed that any of the drag coefficient correction methods presented in their work resulted in poorer values than the original uncorrected data corresponding to a 10% blockage case. Considering also the unknown effects of non-Newtonian rheology on blockage, it was decided not to apply any corrections to the present data.

In general, end effects due to the growth of boundary layers on the side walls of the test section are important. To limit and control their growth and size, Gerich and Eckelmann [35], Stäger and Eckelmann [36] and Norberg [37], amongst others, recommended the use of end plates with specific dimensions. In this work, end plates were not used because the cylinders were close to the inlet of the test section (Section 3.1) hence the tunnel walls behaved like end plates.

Gerich and Eckelmann [35] have shown that a 10 diameters long region close to the edges of a cylinder can be directly influenced by end effects, reducing locally the frequency of vortex shedding. The extent of such region decreases with the Reynolds number according to Stäger and Eckelmann [36]: specifically, for $L/D = 6$ and an end plate of $7.5D$ size, the flow over the cylinder is affected by the side boundary layers for Reynolds numbers below 2700, whereas above 3000–3500 the end effect on the Strouhal number becomes negligible. However, pressure-related quantities are more sensitive and even above $Re \approx 3000$–3500 the end effect is still felt as shown by West and Apelt [32] and Norberg [37]. This

Table 1
Main characteristics of the laser-Doppler anemometer

Laser wavelength	827 nm
Laser power	100 mW
Measured half angle of beams in air	3.68°
Measuring volume size in water (e^{-2} intensity)	
Minor axis	37 μm
Major axis	550 μm
Fringe spacing	6.44 μm
Frequency shift	2.0 MHz

critical Reynolds number increases to 6100–6600 for $L/D = 12$ in the presence of an end plate of $15D$ size.

Williamson [6] reports a second consequence of end effects: events at the ends of the cylinder determine the angle of vortex shedding along the whole cylinder even for aspect ratios larger than 100. This is termed an indirect influence.

3.3. Instrumentation and measuring uncertainties

A diode fibre-optic laser-Doppler system from INVENT, model DFLDA, was used for the velocity measurements, the full description of which can be found in Stieglmeier and Tropea [38]. The S30 optical probe was used together with a 120 mm focusing lens and the LDA main characteristics are listed in Table 1. The output of the avalanche photodiode was processed by a 1990C TSI counter with 2^5 cycles or higher using the single measurement per burst mode and the frequency validation criteria was set to 1% comparison. The large number of cycles was possible since the frequency shift adds N_{sh} fringes to the measuring volume, as given by $N_{sh} = (f_{sh} d_{mcv})/U_p$, where f_{sh} is the shift frequency and d_{mcv}/U_p is the residence time of the particle (d_{mcv}: control volume diameter; U_p: particle velocity) [39]. The frequency information from the counter was sent to a computer via a DOSTEK 1400A interface card for further statistical and numerical analysis. To minimise velocity bias effects the data were acquired at a pre-defined frequency, rather than on the basis of the arrival data rate which was higher than the timer frequency.

The high data rate signal measured downstream of the cylinder was processed by FFT routines in the DOSTEK software to output the vortex shedding frequency. For these measurements, the acquisition frequency was at least five times higher than the frequency of the shedding. These results were confirmed with an independent FFT analysis using the routines of Press et al. [40].

The velocimeter was mounted on a milling table with movement in the three orthogonal directions defined in Fig. 4 and the estimated maximum uncertainties of the mean velocity and frequency measurements were always better than 1.75 and 7%, respectively. The uncertainties were estimated following the procedures outlined by Coleman and Steele [41]. The relative positional uncertainty (uncertainty in locating one measuring point relative to a previous one) was of ±20 μm in the x–z horizontal plane and of ±10 μm in the y-direction, but the uncertainty in positioning the first measuring location relative to the cylinder was ±0.5 mm. All uncertainties quoted in this paper correspond to a 95% confidence level.

4. Fluids characteristics

High and low molecular weight polymers were dissolved in water to produce elastic and weakly elastic shear-thinning fluids, respectively, and the results compared to those of two Newtonian fluids of different viscosity.

The weakly elastic fluids were aqueous solutions of 0.2, 0.3, 0.4 and 0.6 wt.% concentration of a methyl hydroxyethyl cellulose, brand name tylose, grade MH 10,000 K from Hoechst, with a molecular weight of 6000 kg/kmol. The more elastic aqueous solutions were manufactured from carboxymethyl cellulose sodium salt (CMC), grade 7H4C from Hercules, with a molecular weight of 300,000 kg/kmol, at concentrations of 0.1, 0.2, 0.3 and 0.4 wt.%. To prevent bacteriological growth and degradation 0.02 wt.% of the biocide Kathon LXE, grade 1.5%, from Rohm & Haas, was added to all solutions of CMC. The Newtonian fluids were pure tap water and a mixture of 40 wt.% water and 60 wt.% glycerin, having a viscosity of 0.0073 Pa s at 25 °C.

The densities and refractive indices of all non-Newtonian fluids were approximately the same as for water ($\rho = 998\,\text{kg/m}^3$, $m = 1.333$) at 25 °C, whereas for the glycerin–water mixture they were 1148 kg/m^3 and 1.409, respectively.

All the solutions exhibited shear-thinning behaviour as can be seen in the viscosity–shear rate plot of Fig. 6, with the CMC solutions being more shear thinning than the tylose solutions at equal polymer concentrations. The Carreau–Yasuda viscosity model Eq. (1) was fitted to the data and the fittings are represented in the figure by the full lines. Their parameters can be found in Table 2. The power-law viscosity model Eq. (2) was also fitted to the data [42] and the corresponding consistency and power indices are listed in Table 3.

$$\mu = \mu_\infty + (\mu_0 - \mu_\infty)[1 + (\lambda\dot{\gamma})^a]^{n-1/a}, \tag{1}$$

$$\mu = K\dot{\gamma}^{n-1}. \tag{2}$$

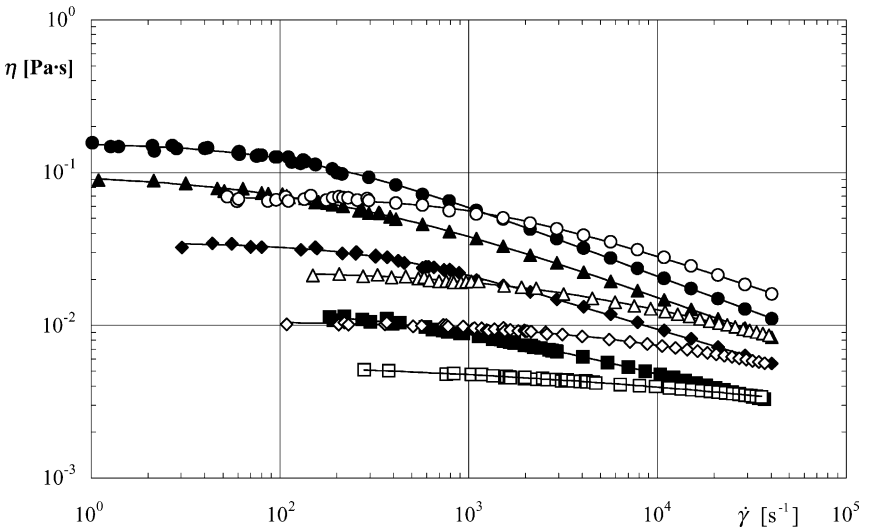

Fig. 6. Viscosity versus shear rate at 25 °C. Full line: adjusted Carreau–Yasuda viscosity model. Symbols as in symbology.

Table 2
Parameters of the Carreau–Yasuda viscosity model for tylose and CMC solutions

Solution	η_0 (Pa s)	η_∞ (Pa s)	λ (s)	a	n	$\dot{\gamma}$ (s^{-1})	Average error (%)
0.4% CMC	0.15983	0.0008	0.06813	0.9909	0.5127	1–4000	0.99
0.3% CMC	0.10181	0.0008	0.04515	0.6343	0.5062	1–4000	1.1
0.2% CMC	0.03579	0.0008	0.02711	1.0431	0.5807	30–4000	1.5
0.1% CMC	0.01367	0.0008	0.01317	0.6671	0.5864	10–4000	0.72
0.6% Tylose	0.07047	0.0008	0.00720	1.0055	0.5584	5–4000	2.1
0.4% Tylose	0.02274	0.0010	0.00304	0.7413	0.6081	10–4000	0.88
0.3% Tylose	0.01074	0.0010	0.00095	0.6531	0.5941	10–4000	0.82
0.2% Tylose	0.00614	0.0008	0.00011	0.2903	0.6311	20–4000	0.53

Table 3
Parameters of the power-law viscosity model for tylose and CMC solutions

Parameters	0.4% CMC	0.3% CMC	0.2% CMC	0.1% CMC	0.6% Tylose	0.4% Tylose	0.3% Tylose	0.2% Tylose
n	0.543	0.583	0.644	0.724	0.580	0.717	0.793	0.880
K (Pa s^n)	0.491	0.268	0.110	0.032	0.526	0.080	0.031	0.009
$\dot{\gamma}$ (s^{-1})			10^2 to 4×10^3				10^3 to 4×10^3	

The elasticity of the solutions was assessed from creep and oscillatory shear test flows. With the creep test, a relaxation time was determined for some of the solutions; they are listed in Table 4 along with the corresponding statistical uncertainty at a 95% confidence level. The relaxation time is the ratio between the shear deformation and the shear rate at a limiting zero shear stress ($\lambda_e = \lim_{\tau \to 0}(\gamma_0/\dot{\gamma}_\infty)$), following the procedure outlined in Bird el al. [43]. Typical results of the creep test, from which the relaxation time was obtained, are shown in Fig. 7 for the 0.4% CMC solution.

The creep tests were repeated twice for the 0.4% CMC and 0.6% tylose solutions to help in the uncertainty analysis, hence the lowest values of statistical uncertainty of 6 and 3% for these fluids, respectively.

Data from the oscillatory tests and further details of the experimental procedure are described elsewhere [44]. Due to the low polymer concentration and the inherent limitations of the rheometer used it was difficult to perform accurate measurements of the storage modulus G'. However, it was possible to determine the ratio between the storage and loss moduli (G'/G'') for the 0.4% CMC solution which at 0.64 was higher than the 0.29 measured for the 0.6% tylose solution.

Table 4
Relaxation time of some solutions from creep test at 25 °C and corresponding uncertainty

	0.4% CMC	0.3% CMC	0.2% CMC	0.1% CMC	0.6% Tylose	0.4% Tylose
λ_e (s)	0.488	0.346	0.162	0.064	0.389	0.053
$\Delta\lambda_e/\lambda_e$ (%)	±6	±10	±14	±18	±3	±19

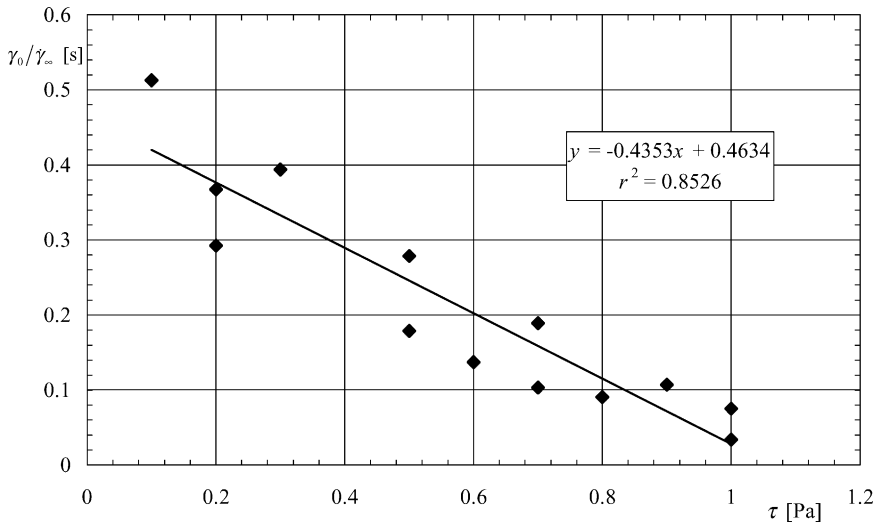

Fig. 7. Determination of the relaxation time for the 0.4% CMC solution using the procedure outlined in Bird et al. [43] based on the creep test.

5. Results and discussion

Results of measurements of the Strouhal number and the formation length for the Newtonian fluids are presented first and compared with data from the literature. Note, however, that the data available in the literature pertain to larger L/D, low free-stream turbulence and low blockage ratio, conditions that are different from those in the present work.

This is followed by a discussion leading to the definition of a characteristic viscosity to be used in the Reynolds number, after which the non-Newtonian results of the Strouhal number and the formation length, and of the various critical numbers marking the onset of different flows regimes, are presented.

5.1. Newtonian fluid results

The Strouhal number ($St = fD/U_\infty$) is plotted in Fig. 8 as a function of the Reynolds number ($Re = \rho DU_\infty/\eta$) for the two cylinders of 10 and 20 mm diameter, where f, D, U_∞, ρ and η stand for the vortex shedding frequency, cylinder diameter, free-stream velocity, density and shear dynamic viscosity, respectively. The broken line represents the Newtonian data of Norberg [37] for infinite aspect ratio cylinder flows with low free-stream turbulence (0.06%), and the full lines delimit the range of values that can be found in the literature, as compiled by Unal and Rockwell [29].

The discrepancies between the measurements and the literature data at $Re < 3000$ are a consequence of the formation of cells with lower shedding frequency at the ends of the cylinder. Norberg [37] has experimentally found the same discrepancies with low aspect ratio cylinders. A more detailed discussion of end effects is postponed to the end of Section 3.2.

For Reynolds numbers of around 3000 and 6000, for the 20 and 10 mm diameter cylinders respectively, the Strouhal number compares well with the literature. These Reynolds numbers correspond to the upper

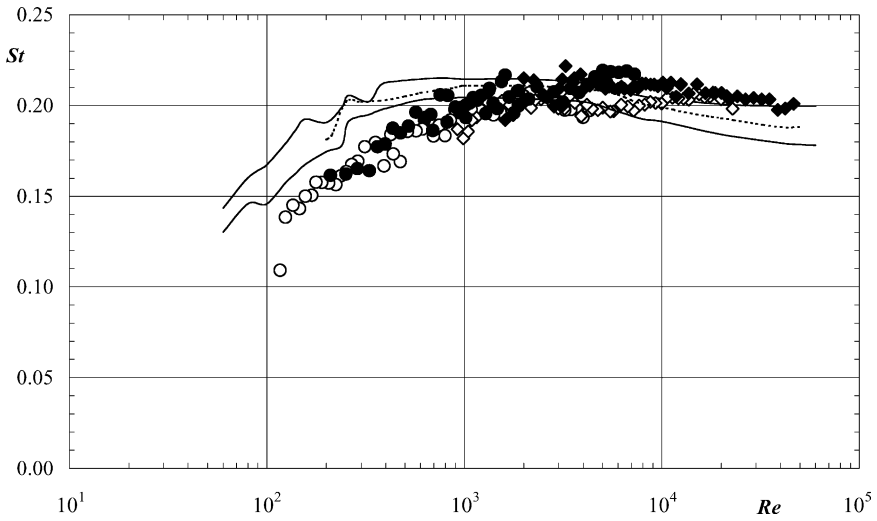

Fig. 8. Variation of the Strouhal number with the Reynolds number for Newtonian fluids. (○, ●) Glycerine and water, (◇, ◆) water; open symbols: 10 mm cylinder; filled symbols: 20 mm cylinder; (—) Unal and Rockwell [29]; (- - -) Norberg [37].

limit of the flow regime affected by the end effects. Within this region, the values of the Strouhal number are less than those of the literature pertaining to non-affected flow, but at higher Reynolds numbers the behaviour is opposite.

If the displacement thickness of the turbulent boundary layer over the test section walls is taken into account, the corresponding total blockage is equal to 10.5% for which the Strouhal number is increased by 0.006 at a Reynolds number of 40,000 [32]. Subtracting this value from the present data, the corrected Strouhal numbers fall within the range defined by Unal and Rockwell [29], except for the smaller diameter cylinder for which the blockage effect is not strong enough to justify the observed differences.

In Fig. 9 the normalised formation length (l_f/D) is plotted as a function of the Reynolds number together with the range of values compiled by [29]. This quantity marks the end of the vortex formation region where the wake stagnation point is located at high Reynolds numbers.

The data clearly show a general decrease of formation length with the Reynolds number. For each cylinder, the glycerin–water mixture flows have larger values of l_f than the pure water, which is in agreement with the findings of Gerrard [7]. This author observed that an increased free-stream turbulence reduced the formation length and the plot of the free-stream turbulence in Fig. 5 confirms the lower turbulence of the more viscous glycerine solution flows.

Generally, at identical Reynolds numbers, the formation lengths are also larger for the smaller cylinder: this is consistent with the lower free-stream turbulence associated with the higher approaching flow velocity required to maintain a constant Reynolds number when reducing the cylinder diameter (by a factor of 2).

At low Reynolds numbers, where end effects are important, the values of l_f/D are larger than those in the literature as found by Norberg [37], who reported increased formation length with small aspect ratio cylinders.

Given the different flow conditions of our experiments and those in the literature, the meaningful comparisons are those between Newtonian and non-Newtonian fluids under similar flow conditions, i.e. with similar levels of free-stream turbulence. Therefore, the Newtonian fluid used henceforth as a

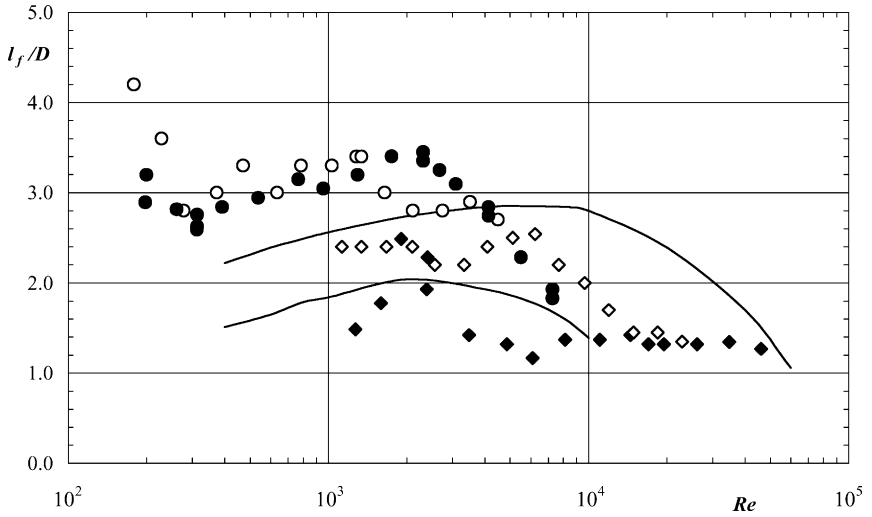

Fig. 9. Variation of formation length as a function of Reynolds number for Newtonian fluids. Symbols as in Fig. 8.

reference is the glycerin–water mixture as it leads to Reynolds numbers and free-stream turbulence of the same order as those pertaining to the non-Newtonian fluids. As will be shown, several issues are raised by the present results and further work must be carried out in the future especially regarding the effect of free-stream turbulence.

5.2. *Selection of Reynolds number*

To define the set of non-dimensional numbers controlling a flow it is necessary to assume a particular class of fluid behaviour or a specific rheological constitutive equation.

The rheological measurements reported in Section 4 and the hydrodynamic behaviour of the same tylose and CMC solutions in other flows confirm that these fluids are viscoelastic and shear thinning [31,45,46]. These characteristics already suggest the need to account for at least three independent fluid material parameters: two quantifying the magnitude of the viscosity and its variation with the shear rate (for example, the power-law, n and k) and a relaxation time for the fluid elasticity [47]. Further rheological evidence and/or the adoption of a particular constitutive equation are essential to be more specific in terms of fluid properties.

Assuming a generalised Newtonian behaviour, the normalisation of the momentum and mass conservation equations produces a Reynolds number and a second non-dimensional quantity involving the derivative of the viscosity relative to the second invariant of the rate of deformation tensor [48]. For the Ostwald-de-Waele power-law model this second number is the power-law index n. The Reynolds number is defined as $Re \equiv \rho U_\infty D/\eta_{ch}$, where the characteristic viscosity η_{ch} is calculated from the fluid rheogram at a characteristic shear rate $\dot{\gamma}_{ch}$.

An appropriate definition of η_{ch} should help to explain and understand the present results. The Reynolds number is proportional to the ratio of inertial and viscous forces; for incompressible Newtonian fluids it is the relevant dimensionless quantity to ensure dynamic similarity, provided there is geometrical similarity. However, for shear-thinning fluids the proportionality between inertial and viscous forces is no longer the

same throughout the flow field when comparing experiments at the same Reynolds number, but differences can probably be minimised for some definitions of the characteristic viscosity.

In this work, the strategy adopted to define the Reynolds number has similarities to that of Metzner and Reed [49] for laminar pipe flow: the minimisation of the differences between the behaviour of the shear-thinning and Newtonian fluids on what concerns the characteristic Reynolds number marking the onset of the laminar vortex shedding regime, Re_{vs}.

According to Gerrard [50], the onset of laminar vortex shedding for flows normal to a flat plate, a rectangular cross-section prism or a circular cylinder occurs at Reynolds numbers (Re_{vs}) between 40 and 70. Thus, Re_{vs} is fairly insensitive to the cylinder geometry, although not to its aspect ratio. The choice of Re_{vs} as the criterion for selecting the correct Reynolds number definition for non-Newtonian fluids is arbitrary because the evidence for Re_{vs} being independent of fluid rheology is scarce. Indeed, the recent numerical calculations of Oliveira [22] for viscoelastic constant viscosity FENE-CR fluids, showed a 6% increase in Re_{vs} due to elasticity, but further research must be carried out on this issue. Still, the reason for adopting this criterion is that the onset of vortex shedding becomes fixed for all fluids, and so the variations in other critical Reynolds numbers result from rheological effects.

The obvious selection of a characteristic shear rate for the cylinder cross-flow is the ratio of the free-stream velocity and the cylinder radius (U_∞/R). This gives rise to a Reynolds number definition referred to as $Re^{\#}$. For Newtonian fluids Gerrard [7] has shown that the main flow characteristics downstream of the cylinder depend on the shear-layer thickness at the end of the formation region and this suggests a second definition of Reynolds number here called Re': since the shear layer originates at the cylinder boundary layer its characteristic shear rate is proportional to that prevailing in the boundary layer. According to White [51] (pp. 281), the wall shear rate in the boundary layer at $\phi = 70^\circ$ from the forward stagnation point represents well the order of magnitude of the predominant shear rate over the entire laminar boundary layer. For practical reasons related to the LDA technique used, we measured instead at $\phi = 75^\circ$ the wall shear rate, to be used in Re'. Two other definitions of characteristic shear rate, were tried and tested leading to Re'', Re^0 (see nomenclature). The procedure to determine the characteristic viscosity for Re'' is presented in detail by Coelho [42] along with a method to estimate $\dot{\gamma}_{w,75^\circ}$ from integral quantities for use with Re'.

Measurements were carried out initially for the 20 mm diameter cylinder for which only the solutions of 0.3 and 0.4% CMC encompassed the transition from the steady laminar to the laminar vortex shedding regimes. Thus, it was based on these measurements that the performance of the various definitions of the Reynolds number were assessed. The measurements with the 10 mm diameter cylinder were used later to draw conclusions as to whether the selected definition of Re lead to a unique Re_{vs}.

Fig. 10 plots the Strouhal number as a function of a fifth Reynolds number (Re^*), to be introduced below, for all fluids and the 20 mm cylinder, but our attention is focused only on the CMC solutions. The transition between both laminar regimes, Re_{vs}, is well shown in the sudden jump in frequency at low Reynolds numbers for the two more viscous CMC solutions, whereas for the 0.2 and 0.1% solutions it was not observed. For the other definitions of Reynolds number, similar plots were drawn but are not shown here for compactness.

The measurements of the shedding frequency f were carried out for both increasing and decreasing free-stream velocity U_∞, but, to avoid a cluttered figure, only the data pertaining to decreasing free-stream velocity is shown in Fig. 10.

In the various plots, Re_{vs} for the 0.3 and 0.4% CMC solutions are either significantly larger or smaller than the Newtonian values from the literature, as will be shown below. For these fluids, Re_{vs} corresponds to

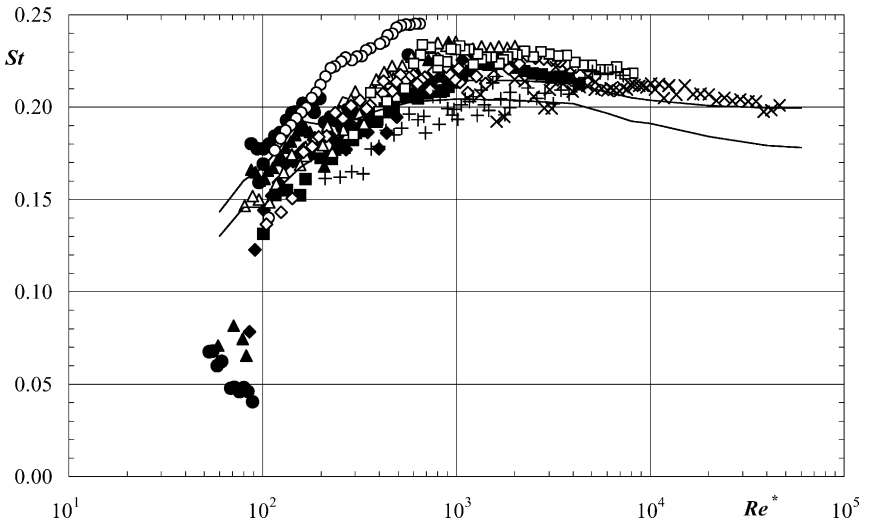

Fig. 10. Variation of the Strouhal number with Reynolds number Re^* for 20 mm cylinder. Symbols as symbology. Full line: Unal and Rockwell [29].

the observed sudden increase in the Strouhal number and this was confirmed by visual inspection of vortex shedding with injection dyes. Note that the lower frequencies measured in the steady laminar regime do not correspond to vortex shedding, but to a small oscillation of the wake which is attached to the cylinder. Since the other Newtonian and non-Newtonian solutions were less viscous, in order to detect the onset of vortex shedding their free-stream velocity would have had to be reduced by a significant amount. This would increase excessively their free-stream turbulence (Fig. 5), thus smearing the power spectral distribution.

Wake stability for Newtonian fluids is known to increase (higher Re_{vs}) with shorter cylinders [37] and from interpolation of the experimental data of Nishioka and Sato [52] it is possible to determine Re_{vs} for specific values of L/D: for $L/D = 6$, $Re_{vs} = 103$ and for $L/D = 12$, $Re_{vs} = 63$. Lee and Budwig [53] gives instead $Re_{vs} = 90$–113 for $L/D = 6$ and $Re_{vs} = 68$ for $L/D = 12$.

For the various Reynolds number definitions, and the 20 mm cylinder, the measured critical Reynolds numbers for the 0.3 and 0.4% CMC solutions were: Re_{vs} (0.3%, 0.4%) = $Re^{\#}_{vs}$ (141, 159); Re'_{vs} (327, 748); Re''_{vs} (215, 424); Re^{0}_{vs} (71, 71). Since none of these definitions resulted in values of Re_{vs} near or within the Newtonian interval of 90–113 for $L/D = 6$, a fifth characteristic shear rate $\dot{\gamma}_{ch}$ was used to force the corresponding Reynolds number (Re^*_{vs}) to be close to 100, a round value approximately in the middle of the corresponding Newtonian range of Re_{vs}. This last definition (see nomenclature) provides values of Re^*_{vs} (100, 100) and is the adopted definition used throughout the remainder of this paper.

With the 10 mm diameter cylinder ($L/D = 12$) the onset of the laminar vortex shedding regime was detected with three solutions of CMC and one solution of tylose, and the corresponding values of Re^*_{vs} are listed in Table 5. Whereas, for the CMC solutions all values of Re^*_{vs} are now lower than for the Newtonian fluids (these Newtonian reference data are from [52,53]), for the 0.6% tylose Re^*_{vs} is basically the same. This different behaviour of CMC and tylose could be linked to end effects and this is related to fluid elasticity. On other occasions, different behaviour between these two distinct polymer solutions were detected when the cylinder diameter was changed, and flow visualisations have confirmed a peculiar end effect for the CMC solutions [54].

Table 5
Onset of the laminar vortex shedding regime for the 10 mm cylinder ($L/D = 12$)

Fluid	Re_{vs} based on Re^*
0.4% CMC	53
0.3% CMC	49
0.2% CMC	43
0.6% Tylose	69
Newtonian fluid (Nishioka and Sato [52])	63
Newtonian fluid (Lee and Budwig [53])	68

The St versus Re^* plots in Figs. 10 and 11, the latter plotting the same data vertically shifted, show similar trends for all fluids with the data falling in the vicinity of the curves of Unal and Rockwell [29] for infinite aspect ratio cylinders. Increased polymer concentration raises the frequency shedding for each polymer and, in general, the non-Newtonian solutions have higher Strouhal numbers than the Newtonian fluids.

This last observation is in contradiction with previous findings for non-Newtonian fluids [15,18,19]. Note that Gadd [15] worked with elastic fluids of constant viscosity and the remaining works concern weakly shear-thinning fluids, but all are basically Boger fluids. The reason for this apparent discrepancy, which has not been previously described in the literature as far as we are aware, is explained by the following: in laminar flow, shear thinning reduces the boundary layer thickness [55,56] and, by implication, the diffusion length, which increases the Strouhal number [54].

In the next section, the transitions between the various flow regimes are analysed and described in detail. The investigation on the detailed characteristics within each flow regime is left to the second part of this work [54].

Before proceeding, however, it is important to emphasise the good reproducibility of the data in the current experimental program which took several years and can be assessed in Fig. 1.

5.3. Delimitation of flow regimes

The variations of Strouhal number and formation length with the Reynolds number, aided by power spectra of velocity fluctuations, allow the identification of the various flow regimes. These are defined on the basis of the same criteria and flow characteristics that separate flow regimes with Newtonian fluids.

Not all flow regimes are observed with all solutions because of their different viscosities and the difficulties of measuring at low Reynolds, where the free-stream turbulence becomes too high. This task will benefit by looking first at a fluid where the various regimes are clearly identified, as is the case of the 0.2% CMC flow around the 20 mm cylinder.

Data pertaining to measurements taken with increasing and decreasing free-stream velocity are presented first, henceforth referred to as decreasing and increasing curves, respectively. It is helpful to combine on the same plot the vortex shedding frequency and formation length data, as is done in Fig. 12.

The power spectral distributions shown in Fig. 13 were taken at $x = 4D$ and $y = -0.75D$ (see Fig. 4 for co-ordinate system) and were used to determine the shedding frequency, as explained in Section 3.3. Fig. 13 only shows a few representative spectra for a single fluid.

The last element of the analysis is the variation with Reynolds number of the average streamwise turbulence ($\overline{u'}$) in the near-wake symmetry plane. For each Reynolds number the profile of streamwise

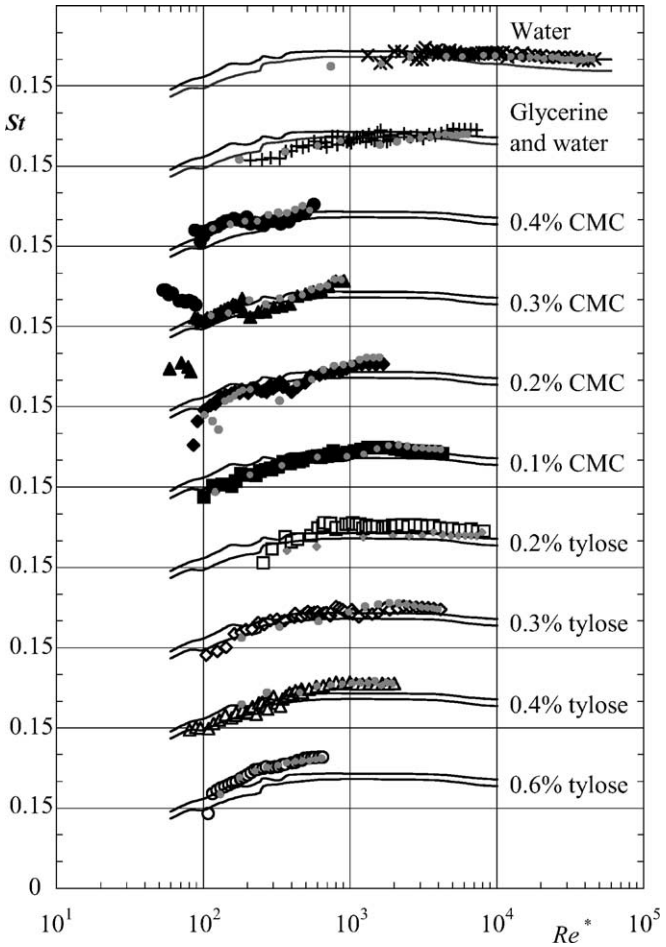

Fig. 11. Reproducibility of the *St* measurements for the 20 mm cylinder. Grey symbols from Coelho et al. [57]; full line: Unal and Rockwell [29].

normal Reynolds stress ($\overline{u'^2}$) was measured along the near-wake symmetry plane (from the rear stagnation point to around $x/D = 5$). The ensemble average of the N measured values of $\sqrt{\overline{u'^2}}$ is the average streamwise turbulence, $\overline{u'}$ (see nomenclature).

Differences between the increasing and decreasing Strouhal number curves in Fig. 12 are small; the irregular pattern in the range $200 < Re^* < 500$ and the formation length sudden drop for $Re^* > 360$ are the most relevant findings. In this range of Reynolds numbers and for Newtonian fluids, Chyu et al. [58] and Prasad and Williamson [30] found that the vortices are turbulent and the laminar-turbulent transition takes place in the shear layer, moving towards the cylinder as the Reynolds number further increases. Bloor [8] refers the 1953 work of Roshko, who found that the transition regime, which follows the laminar shedding regime, extended to a Reynolds number of 300, being characterised by irregular violent bursts of velocity in the wake and an irregular shedding frequency. Roshko found again regular shedding with a well-defined frequency at higher Reynolds numbers between 300 and a critical value of about 3×10^5.

Similar findings are also reported by Norberg [37] who stated that "the shedding frequency at Reynolds numbers lower than 5000, except within the transition regime (approximately $160 < Re < 250$), is extremely narrow-banded whereas at higher Reynolds numbers in the (upper) subcritical regime, the shedding frequency is time dependent and has a significantly higher relative bandwidth."

Next, the methodology used to quantify the various critical Reynolds numbers for all Newtonian and non-Newtonian fluids is described. The criteria are the same as above for Newtonian fluids, in the literature.

For each fluid, there are two sets of power spectral distributions: one for ascending and the other for descending free-stream velocity. From their inspection, it is possible to identify two sets of consecutive Reynolds numbers where there is a specific variation of the spectra in the region of the peak vortex shedding frequency, such as: from a sharp to a less sharp or non-existing peak or from a broad to a narrow peak. Thus, for each transition there are four Reynolds numbers and their ensemble average defines the corresponding critical Reynolds numbers.

The specific transitions defining the various critical Reynolds numbers are:

- Re^*_{otr}, transition from a clear to a less clear or non existing peak, it represents the onset of the transition regime;
- Re^*_{etr}, transition from a less clear or non-existing peak to a clear peak, it represents the end of the transition regime;
- Re^*_{bbp}, transition from a broad band to a narrow peak frequency.

The critical Reynolds number Re^*_{lf} was determined from plots showing the variation of l_{f} with Re^* (such as Fig. 12) and corresponds to the sudden drop in l_{f}. It indicates the onset of the shear-layer transition regime when Re^*_{lf} is larger than Re^*_{etr}.

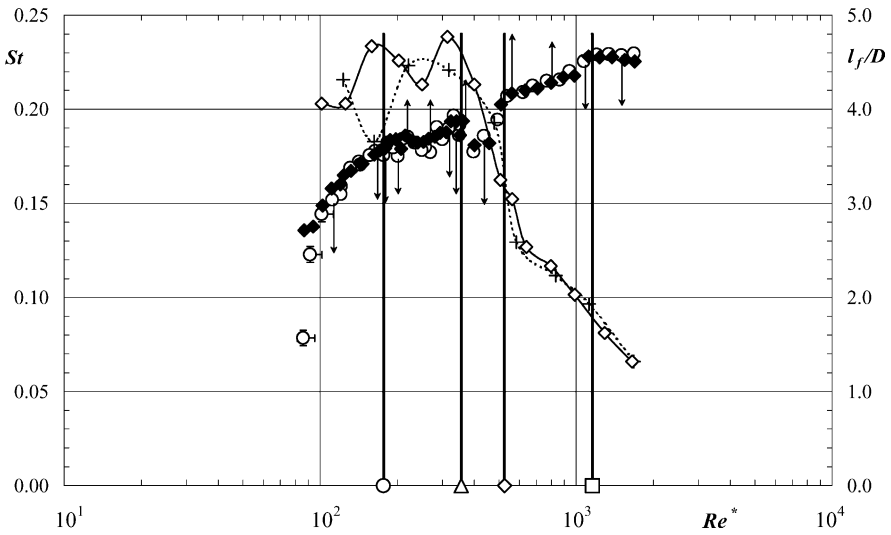

Fig. 12. Variation of the Strouhal number (St) and normalised formation length (l_{f}/D) with the Reynolds number for 0.2% CMC, 20 mm cylinder. (○) St descending curve; (◆) St ascending curve; (+) first measurement of l_{f}/D; (◇) second measurement of l_{f}/D; vertical lines: (○) end of laminar regime; (△) beginning of strong decrease in l_{f}/D; (◇) end of transition regime; (□) end of region with a very wide spectral distribution. (I, H) Uncertainties in the values of St and Re^*.

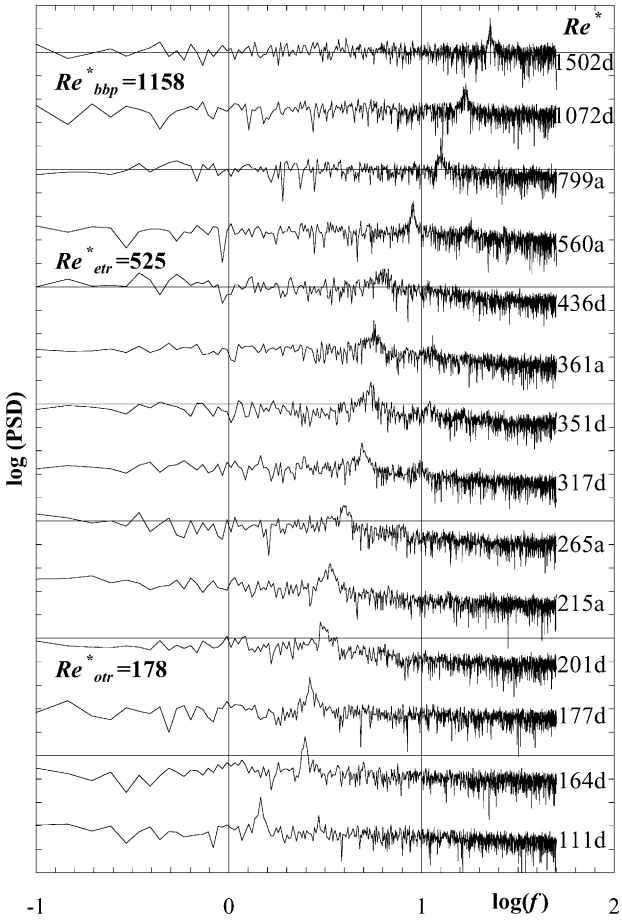

Fig. 13. Variation of the power spectral distribution with frequency for the 0.2% CMC solution at various Reynolds numbers. The suffixes (a/d) refer to the data obtained while increasing/decreasing the free-stream velocity.

For the 0.2% CMC data, this process lead to the following conclusions:

(i) Up to Re^* of 178 (the average value of 185 and 172 pertaining to increasing and decreasing data, respectively) the peak frequency is well defined and very sharp, an indication that vortex shedding is laminar.

(ii) In the range $178 < Re^* < 525$ the peak frequency broadens and exhibits some perturbations. This regime can be separated into two sub-regions, namely $178 < Re^* < 360$ and $360 < Re^* < 525$. At the upper sub-regime the peaks in the power spectra have a broader base and are less clear than those in the lower sub-regime, Fig. 13. The transition between the two sub-regimes is characterised by a sudden decrease in the Strouhal number (Fig. 12 at $Re^* \approx 360$), which is typical of small-scale instabilities combined with intermittent vortex dislocations. This is further confirmed by the peak in the rms of the velocity fluctuations measured at the wake of the cylinder in the upper sub-regime range and marked by an arrow in Fig. 14. Thus, the transition regime starts at $Re^* = 178$ and ends at $Re^* = 525$ for the 0.2% CMC solution.

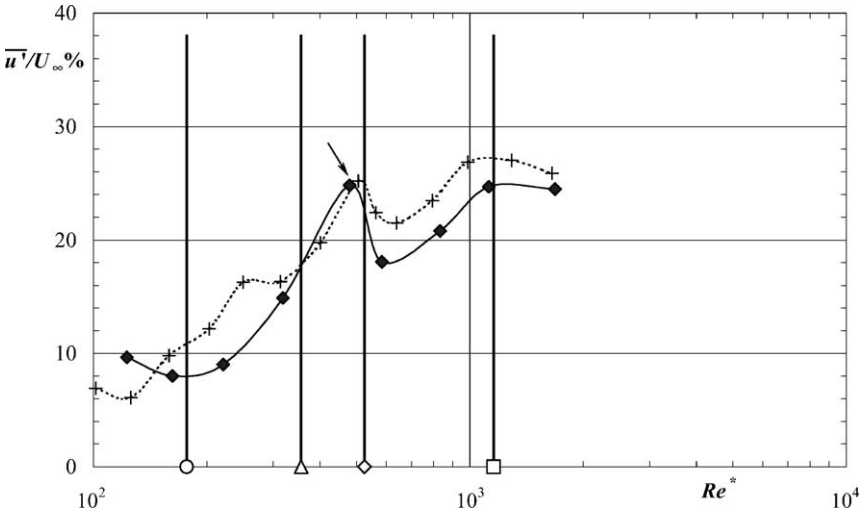

Fig. 14. Average rms of the axial velocity measured along the centreline in the near wake of the 20 mm cylinder, 0.2% CMC. (◆) First measurement of u'/U_∞; (+) second measurement of u'/U_∞; vertical lines: (○) end of laminar regime; (△) beginning of strong decrease in l_f/D; (◇) end of transition regime; (□) end of region with a very wide spectral distribution.

(iii) Within the transition regime, the velocity spectra in Fig. 13 show hysteresis: the curve for $Re^* = 351$d (d refers to decreasing Re) has a broader peak than the increasing curve ($Re^* = 361$a). This difference is consistent with a flow condition obtained from, in the former case, a decrease in free-stream velocity coming from the perturbed upper region ($360 < Re^* < 525$), where there are disturbances and dislocations and, in the latter case from an increase in free-stream velocity from a less perturbed flow condition;

(iv) An unexpected result, from a Newtonian perspective, was the strong decrease in formation length at $Re^* \approx 360$, well before the end of the transition regime. For Newtonian fluids, l_f decreases at much higher Reynolds numbers, within the shear-layer transition regime, which for the 0.2% CMC would be for $Re^* > 525$. On the contrary, with the tylose solutions the behaviour is the same as for Newtonian fluids, with the decrease in l_f occurring at Reynolds numbers beyond the transition regime.

(v) So, the flow at $Re^* = 525$ is already in the shear-layer transition regime and for $Re^* > 525$ the spectra of the velocity fluctuations exhibit again well-defined, narrow peaks, as in the four upper curves of Fig. 13.

(vi) At Reynolds numbers well above those marking the end of the transition regime, the base of the peak frequency becomes progressively narrower ($Re = 1072$d and 1502a in Fig. 13). This is possibly due to a modification of the end effects observed at a Reynolds number of about 1150. In fact, the two St–Re^* curves for the 10 mm cylinder in Fig. 15, show agreement only for Reynolds numbers above Re^*_{bbp}, those for which the spectra has a very narrow base at peak frequency. These critical Reynolds numbers for the two experiments are marked in the figure by vertical lines and are lower than those pertaining to the 20 mm cylinder. Although small, the differences between the two data sets are consistently constant at low Reynolds numbers; this could be due to differences in vortex shedding angle which is related to end effects.

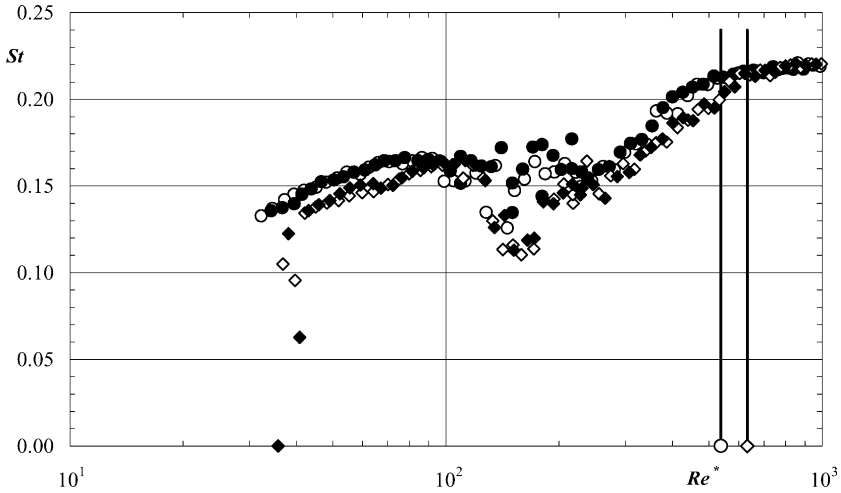

Fig. 15. Variation of the Strouhal number with the Reynolds number for 0.2% CMC flow around the 10 mm cylinder. Set 1: (●, ○); Set 2: (◆, ◇); ascending data: open symbols; descending data: filled symbols; vertical lines mark the end of the region where the peak frequency has a broad distribution.

A similar data analysis was carried out for all fluids and both cylinders in order to extract the corresponding information on the limits of the various flow regimes. The result of this extensive analysis is summarised in Tables 6 and 7 for the 20 and 10 mm cylinder, respectively, in terms of Re^*. Together with Re^*_{lf}, the corresponding values of l_f/D are also listed in those tables.

These data show that the characteristic Reynolds numbers decrease when L/D increases in agreement with the available Newtonian data. The relative variations of the various critical Reynolds numbers with L/D are similar to that reported in the Newtonian literature for Re^*_{vs}. Note the scarcity of Newtonian literature on the effect of L/D on the other critical Reynolds numbers.

The difference between Re^*_{otr} and Re^*_{etr} ($\Delta Re^* \equiv Re^*_{etr} - Re^*_{otr}$) quantifies the extent of the transition regime, which is reduced with polymer concentration. For the 0.6% tylose solution it was not even possible to detect this flow regime.

Table 6
Critical Reynolds numbers marking the onset or the end of flow regimes (20 mm cylinder)

Fluid	Re^*_{otr}	Re^*_{etr}	$Re^*_{lf} - (l_f/D)$	Re^*_{bbp}
0.4% CMC	165 (±9.0%)	316 (±12.1%)	275 (±7.0%) − 4.4	416 (±26.4%)
0.3% CMC	163 (±8.9%)	419 (±9.5%)	271 (±5.6%) − 4.3	676 (±23.90%)
0.2% CMC	178 (±8.9%)	525 (±9.2%)	356 (±6.3%) − 4.5	1158 (±10.4%)
0.1% CMC	355 (±13.1%)	1209 (±16.1%)	663 (±13.3%) − 3.0	1730 (±10.1%)
0.6% Tylose	Not detected	Not detected	175 (±3.7%) − 3.8	415 (±11.9%)
0.4% Tylose	143 (±13.3%)	555 (±9.9%)	1094 (±2.5%) − 2.7	1488 (±11.3%)
0.3% Tylose	Hard to detect	1160 (±11.5%)	1852 (±3.9%) − 2.9	2372 (±8.8%)
0.2% Tylose	Hard to detect	2062 (±9.6%)	1945 (±8.3%) − 2.3	4103 (±12.4%)
Glycerin + water	717 (±12.5%)	1886 (±11.8%)	2000 (±7.1%) − 3.4	5271 (±10.6%)

Table 7
Critical Reynolds numbers marking the onset or the end of flow regimes (10 mm cylinder)

Fluid	Re^*_{otr}	Re^*_{etr}	$Re^*_{lf} - (l_f/D)$	Re^*_{bbp}
0.4% CMC	118 (±3.2%)	208 (±3.6%)	160 (±8.6%) − 6.6	Always wide
0.3% CMC	117 (±11.4%)	241 (±8.7%)	167 (±7.9%) − 6.2	Always wide
0.2% CMC	98 (±8.7%)	433 (±10.2%)	212 (±6.5%) − 6.1	538 (±6.4%)
0.1% CMC	149 (±6.8%)	667 (±13.4%)	487 (±13.2%) − 3.2	1573 (±30.7%)
0.6% Tylose	Not detected	Not detected	100 (±7.8%) − 6.4	Always wide
0.4% Tylose	139 (±11.6%)	456 (±6.0%)	660 (±8.5%) − 3.0	980 (±9.4%)
0.3% Tylose	Hard to detect	1101 (±4.9%)	1279 (±12.6%) − 2.5	1472 (±6.1%)
0.2% Tylose	Hard to detect	1149 (±13.6%)	1844 (±7.5%) − 2.3	3229 (±7.5%)
Glycerin + water	361 (±13.8%)	1400 (±11.8%)	1337 (±6.8%) − 3.4	2563 (±6.7%)

To understand the influence of fluid properties on the critical Reynolds numbers, we emphasize the need for comparisons under the same geometrical conditions, i.e. the same L/D and end plates/cylinder diameters ratio. However, some quantities, such as ΔRe^*, are less geometry dependent: for the glycerine–water solution the variation of ΔRe^* with L/D is equal to 13%, i.e. of the same order of magnitude as the uncertainties in measuring Re^*_{otr} and Re^*_{etr}.

In general, for each type of additive and cylinder diameter, an increase in polymer concentration lowers the critical Reynolds numbers. In these comparisons, the glycerin–water mixture must be viewed as a 0% polymer concentration case. The reductions of Re^*_{etr}, Re^*_{lf} and Re^*_{bbp} are attributed to fluid elasticity rather than to shear thinning: the solutions of 0.2–0.4% CMC show similar levels of shear thinning (power indices of 0.64, 0.58 and 0.54, respectively) but in contrast, the relaxation time of the 0.4% CMC solution is three times higher than that of the 0.2% CMC and so the critical Reynolds numbers for 0.4% CMC are well below those for 0.2% CMC.

The advance of flow regimes by fluid elasticity was previously observed by White [59] and Sarpkaya et al. [14]. Cadot and Kumar [19] have also seen that elasticity can inhibit the formation of large-scale three-dimensional structures, especially those pertaining to the vortex shedding A-mode, therefore advancing the end of the transition regime. Thus, elasticity lowers Re^*_{etr} as well as the values of the other higher critical Reynolds numbers. In contrast, the analysis of the stability curves of Acharya et al. [60] has shown a delay in the transition of regime due to enhanced shear thinning. More recently, D'Alessio and Pascal [61] reported a shear-thinning dependent increase of the critical Reynolds number at which the recirculation bubble first appears downstream of the cylinder. So, the literature also suggests that elasticity and shear thinning have opposite effects upon the variation of the critical Reynolds numbers.

In the laminar shedding regime the frequency increases with polymer concentration because the fluids become more shear thinning. A higher shedding frequency implies a larger number of vorticity filaments and, since these are precursors of the transition [19], there is a direct relationship between the decrease in Re^*_{otr} and additive concentration. However, the variation is non-linear and Re^*_{otr} asymptotes at higher polymer concentrations.

Given the differences in free-stream turbulence between this and other works in the literature, it is necessary to emphasize at this stage that the free-stream turbulence is fairly constant for the various Newtonian and non-Newtonian flows being compared and that it does not seem to have any significant

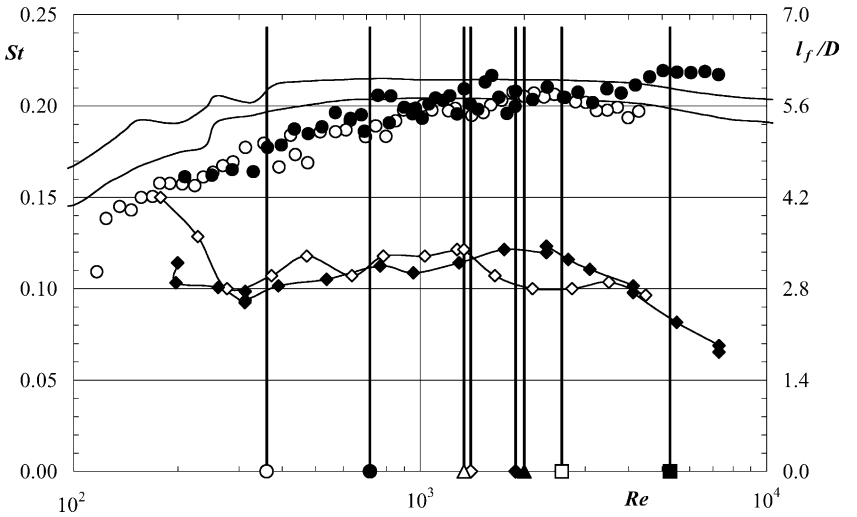

Fig. 16. Strouhal number (○, ●) and the l_f/D (◇, ◆) curves for the 10 and 20 mm cylinders with glycerin–water mixture. Open symbols: 10 mm; filled symbols: 20 mm; vertical lines: (○, ●) Re_{otr}; (◇, ◆) Re_{etr}; (△, ▲) Re_{lf}; (□, ■) Re_{bbp}.

influence on the variations of critical Reynolds numbers. For example, the pairs (turbulence; Re^*_{etr}) for the solutions of 0.4, 0.3 and 0.2% of tylose, measured for the 20 mm cylinder, are: (3.5%, 555), (3.7%, 1160) and (3.5%, 2062), respectively. So, for identical levels of free-stream turbulence, Re^*_{etr} increases by a factor of 4 when polymer concentration is halved. In any case, further research is required to investigate in detail the effects of free-stream turbulence on non-Newtonian cylinder flow characteristics.

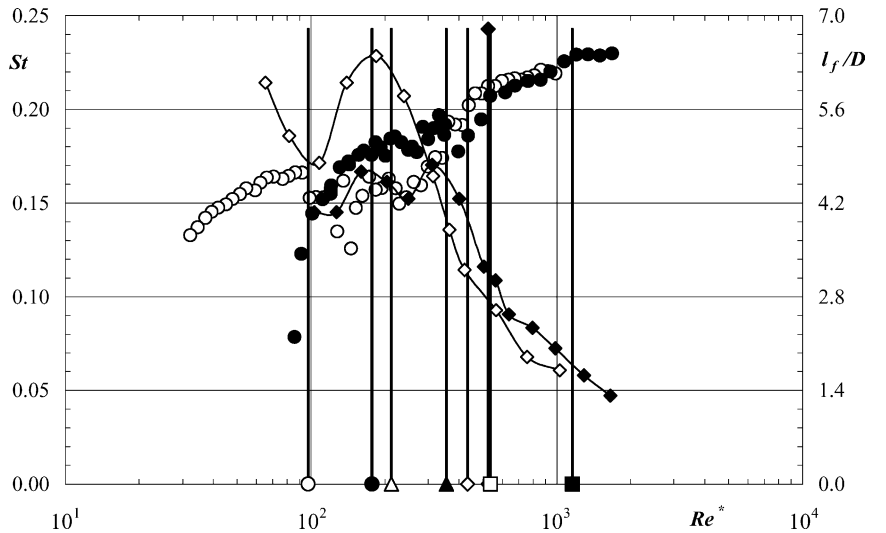

Fig. 17. Strouhal number and the l_f/D curves for the 10 and 20 mm cylinders with the 0.2% CMC solution. Symbols as in Fig. 16.

5.4. Other diameter effects

The effect of cylinder diameter on the variations of St and l_f with Reynolds number is similar for all solutions, therefore only the results pertaining to the viscous Newtonian fluid and the 0.2% CMC solution are presented in Figs. 16 and 17, respectively.

Regarding the formation length, the effect is stronger with the non-Newtonian fluid than with the glycerin–water mixture. In both cases, l_f/D for the larger cylinder is higher than for the smaller cylinder in the region of rapid decrease of l_f/D, as was also observed by Norberg [37] for Newtonian fluids at $Re = 1.5 \times 10^3$.

Regarding the Strouhal number, St is slightly higher for the larger cylinder within the transition regime, and this is consistent with the inversely proportional relationship between formation length and vortex shedding frequency studied in Section 2: at identical values of l_f/D the larger blockage of the 20 mm cylinder will increase the Strouhal number.

6. Effect of elasticity

In the previous section, we have seen that the transition between the various flow regimes could not be simply explained on the basis of viscous properties. These were quantified by the intensity of shear thinning (power-law index) and a Reynolds number, Re^*, where the viscosity was calculated at a mean flow characteristic shear rate. In this section, the effect of elasticity on the transitions of regime is analysed.

Elasticity can be quantified with various non-dimensional numbers. Here, the Weissenberg number ($We \equiv \lambda_e U_\infty / D$), representing the ratio of elastic and viscous forces is used. In a non-viscometric flow it is also useful to use the reciprocal of the first elastic number (El_1) defined by Astarita and Marrucci [47]

$$\frac{1}{El_1} \equiv \frac{D^2 \rho}{\eta_{ch} \lambda_e} \equiv \frac{Re}{We}. \tag{3}$$

This quantity is a ratio between inertia and elastic forces and can also be calculated as the ratio of Re and We, a notation that is used here preferentially.

6.1. The transition regime

Figs. 18 and 19 show the variations of Re^*_{etr} and ΔRe^* with the Weissenberg number, respectively. The figures include data for 0.3 and 0.2% tylose solutions, for which the relaxation time λ_e could not be measured in the creep test but had to be estimated on the basis of Fig. 23; this alternative determination of λ_e is explained at the end of Section 6.2.

Fig. 18 shows well the advance of the end of the transition regime with the Weissenberg number. Since Re^*_{etr} decreases at a faster rate than Re^*_{otr}, the extent of the transition regime is also reduced with increased elasticity, as shown in Fig. 19. In Coelho and Pinho [54], who analyses in detail the flow characteristics within each flow regime, this phenomenon is explained.

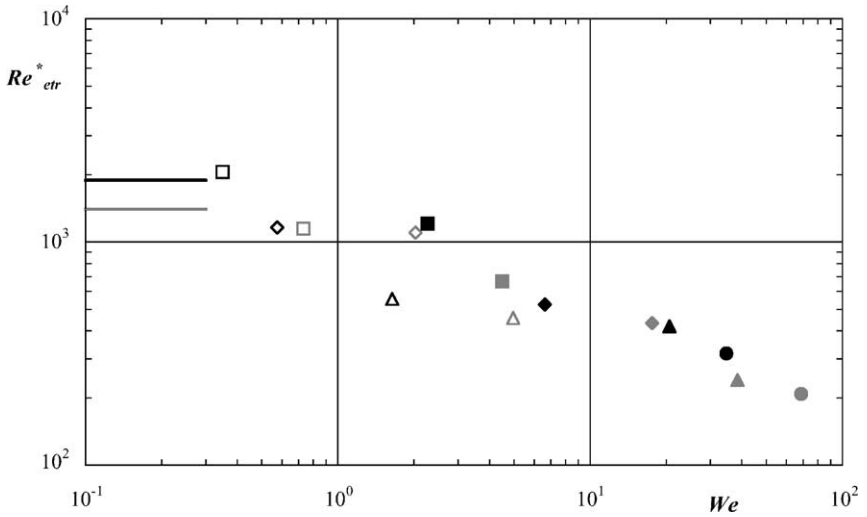

Fig. 18. Variation of the end of transition regime, Re^*_{etr}, with the Weissenberg number (black symbols: 20 mm cylinder; grey symbols: 10 mm cylinder). Symbols as in symbology. Horizontal lines: Newtonian data.

6.2. Re/We and characteristic shear rates

Radial measurements of the tangential velocity component at $\phi = 75^\circ$ from the forward stagnation point allowed the quantification of the normalised boundary layer thickness (δ/s). Here, δ is the radial distance measured from the cylinder wall up to the location where $\partial u/\partial r = 0$ and s is the arc length measured from the forward stagnation point, $s = \phi D/2$. The variation of the boundary layer thickness with the Reynolds number (Re^*) is shown in Fig. 20. The solid line represents the Blasius prediction for

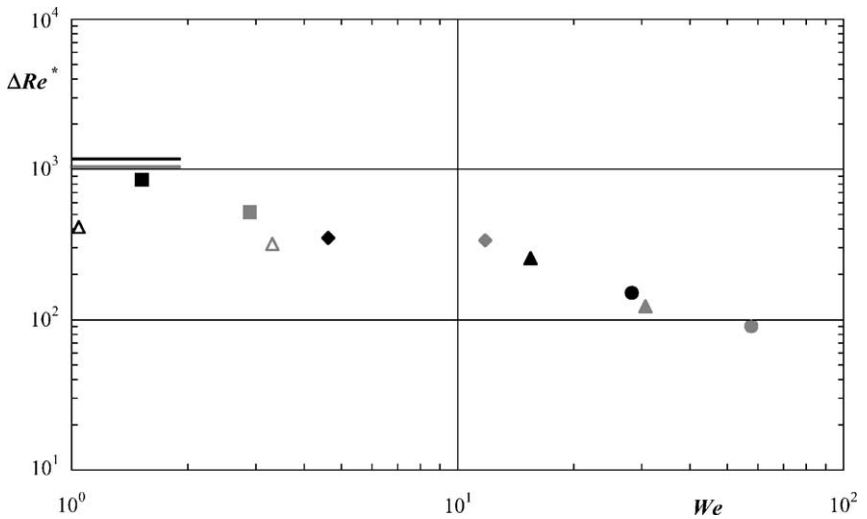

Fig. 19. Variation of the range of transition regime $\Delta Re^* = Re^*_{etr} - Re^*_{otr}$, with the Weissenberg number (black symbols: 20 mm cylinder; grey symbols: 10 mm cylinder). Symbols as in symbology. Horizontal lines: Newtonian data.

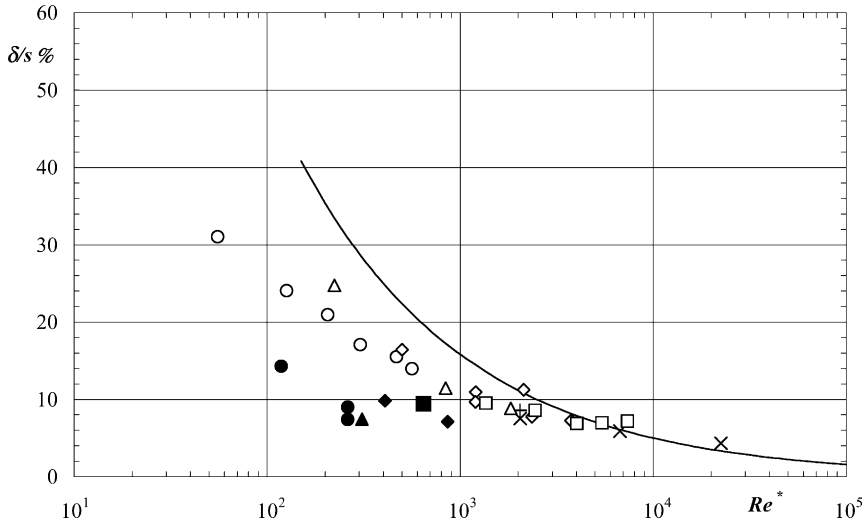

Fig. 20. Variation of the thickness of the boundary layer at $\theta = 75^\circ$ with the Reynolds number (Re^*) for the 20 mm cylinder. Symbols as in symbology. Full line: Blasius equation.

a Newtonian plane laminar boundary layer with a zero pressure gradient and is shown here and in Fig. 21 only to help in the comparisons.

The variation of δ/s is as expected in the absence of any transitional influence decreasing with polymer concentration, especially at low Reynolds numbers. With CMC the boundary layer thickness is thinner than with tylose.

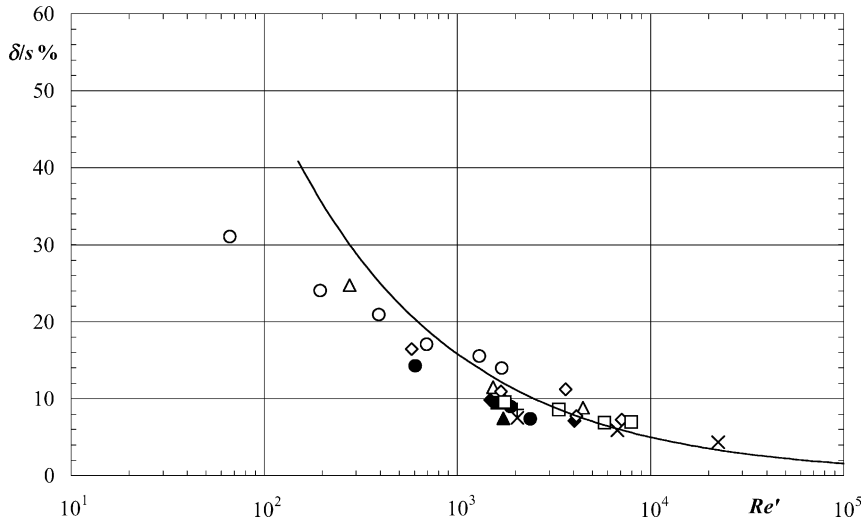

Fig. 21. Variation of the thickness of the boundary layer at $\theta = 75^\circ$ with the Reynolds number (Re') for the 20 mm cylinder. Symbols as in symbology. Full line: Blasius equation.

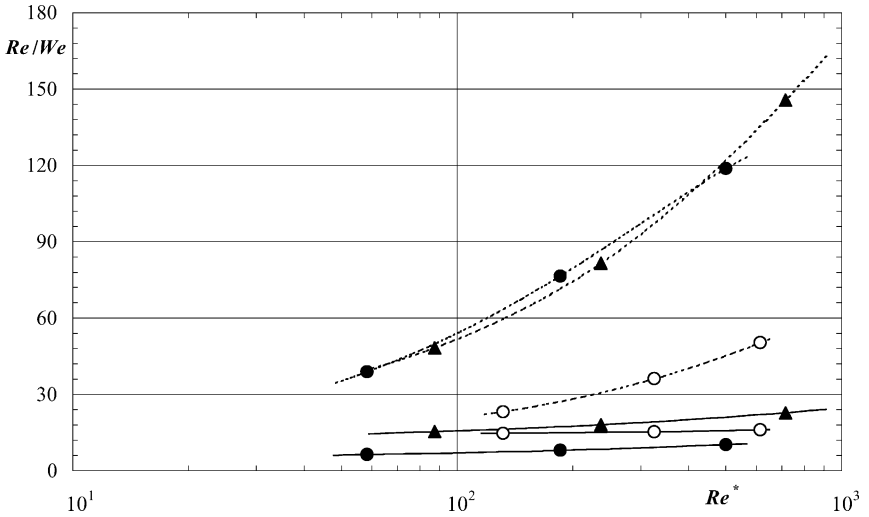

Fig. 22. Variation of the elastic numbers Re^*/We (—) and Re'/We (- - -), with the Reynolds number (Re^*). Symbols as in symbology.

Plotting δ/s as a function of Re' in Fig. 21 (Re' uses local wall viscosity) shows a better agreement between the various sets of data, as expected. This is so because the boundary layer behaviour is controlled by local high shear rates rather than by shear rates representing average flow characteristics over the cylinder, such as $\dot{\gamma}_{ch} = U_\infty/(2D)$ appearing in Re^*.

The variations of Re^*_{etr} and $\Delta Re'$ were also represented as a function of the two different elastic numbers Re'/We and Re^*/We and in all cases a decrease with elasticity was observed, thus confirming the conclusions in Section 6.1.

In an attempt to determine whether there was a preferred non-dimensional number to quantify elasticity, the variations of the critical Reynolds numbers with several elastic numbers were analyse. The fittings of the critical Reynolds numbers with Re'/We were consistently better correlated and especially so in comparison with the fitting using Re^*/We.

For several of the fluids, the variations of Re^*/We and Re'/We with Re^* are plotted in Fig. 22. The data show that, the 0.6% tylose solution has the highest ratio of elastic and inertia forces when using Re'/We, i.e. at locations where very high shear rates are predominant such as in the boundary layer.

In Section 5.3, it was found that 0.6% tylose did not show any signs of the transition regime and fluid elasticity was found to shorten the extent of the transition regime. These findings are consistent with the relative position of the various fluids in Fig. 22, when using the non-dimensional number Re'/We to quantify elasticity. This means that both the end of the transition regime and its extent are sensitive to the highest shear rate in the flow field as well as to the ratio between inertia and elastic forces (Re/We). Since for constant viscosity fluids Re/We is not so clearly dependent on local shear rates, the use of a Boger fluid would not allow a proper investigation of the influence of high shear rates and of Re/We upon the macroscopic cylinder flow characteristics.

According to the linear stability analysis of the two-dimensional roll-up instability of Azaiez and Homsy [62]: "... The Oldroyd-B model was studied in the limit that the Weissenberg number and the Reynolds number, approach infinity while the ratio We/Re remains finite. In this limit, the effect of elasticity is focused on the purely inertial instabilities modes. The analysis reveals that the range of

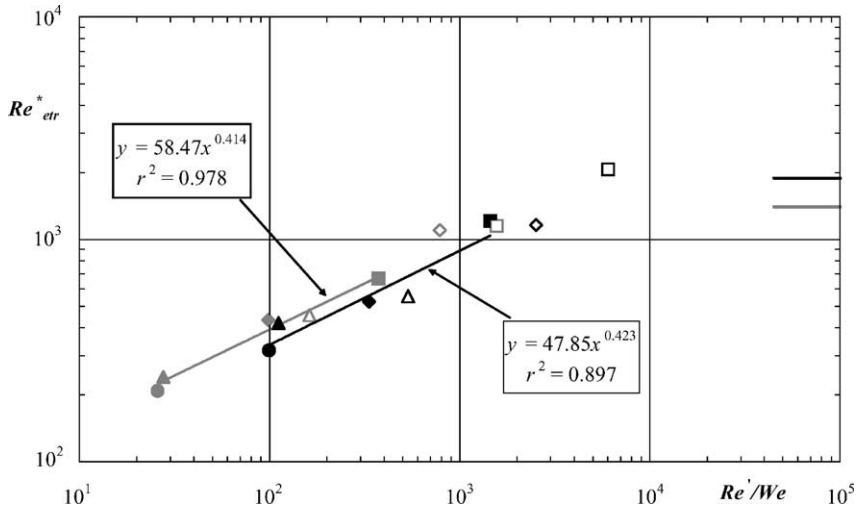

Fig. 23. Variation of the end of transition regime, Re^*_{etr}, with the elastic number Re'/We (black lines and symbols: 20 mm cylinder; grey lines and symbols: 10 mm cylinder). Symbols as in symbology. Horizontal lines: Newtonian data.

unstable wavenumbers and maximum growth rate decrease as the ratio We/Re increases, indicating both damping of small scales and stabilisation of the roll-up relative to the Newtonian case." From the evolution of St with Re^* of Fig. 10, it looks as though this stabilisation of the two-dimensional roll-up has taken place for the 0.6% tylose solution.

Kumar and Homsy [63] have also numerically investigated how the addition of small amounts of polymer affects the sequence of hydrodynamic instabilities leading to turbulence in free shear layers. They found that the polymers would have to inhibit transition to turbulence in free shear layers by interfering with the roll-up process. This interference looks obvious with the 0.6% tylose solution. In contrast, in their discussion of high Reynolds number flows, which have an extensional motion superimposed on a mean shear motion, they consider that the extensional motion will stretch the polymers and produce large elastic stress gradients. The resulting competition between elastic and inertial forces may then lead to significant flow modification.

Given the apparent physical relevance of Re'/We, the relationship between Re^*_{etr} and elasticity is plotted in Fig. 23 as a function of Re'/We and a power law is fitted to the data. Since the effect of L/D is different for each cylinder size, it is better to correlate separately the data for the two cylinders, as in Fig. 23. Here, the 0.2 and 0.3% tylose data were not used because there was no independent determination of λ_e for these fluids. In fact, given the good correlation of this power law fit, this figure was used instead to estimate the relaxation times of these two fluids and the corresponding data added later to the figure (symbols (□) and (◇)). The numerical values of λ_e for the 0.3 and 0.2% tylose solutions estimated in this way were of 0.0212 and 0.0165 s respectively, which are lower than the 0.06 s measured in the creep tests of Section 4 for the 0.4% tylose solution.

6.3. *Variation of Re^*_{bbp} with elasticity*

Finally, the variation with elasticity of the critical Reynolds number marking the end of the broad base peak in the power spectra (Re^*_{bbp}) is plotted in Fig. 24. The figure shows the advance of Re^*_{bbp} with

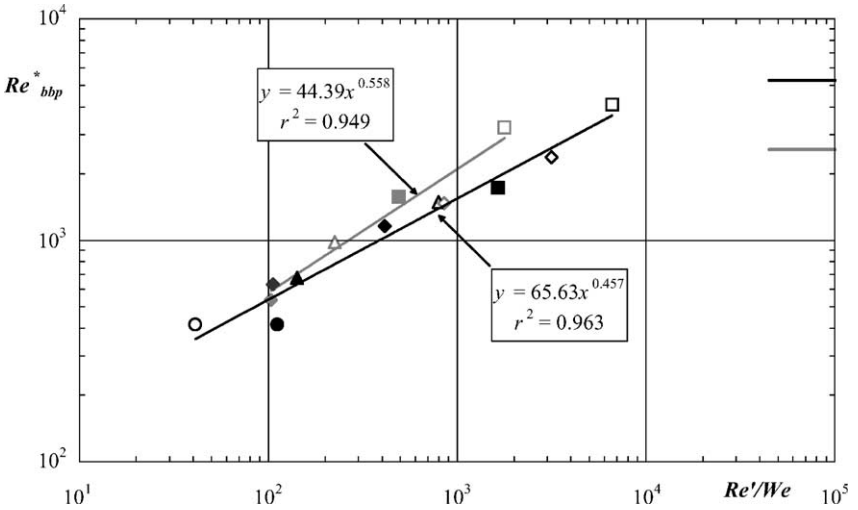

Fig. 24. Variation of the Reynolds number where a broad basis at the peak frequency, Re^*_{bbp} first occurs with the elastic number Re'/We (black lines and symbols: 20 mm cylinder; grey lines and symbols: 10 mm cylinder). Symbols as in symbology. Horizontal lines: Newtonian data.

elasticity for both cylinders, at a rate which is larger than that for Re^*_{etr}. Thus, elasticity reduces the extent of the regime comprised between Re^*_{etr} and Re^*_{bbp}.

Since the meaning of the change from a broad to a narrow peak in the power spectra is still open to discussion, we can not be fully conclusive on this issue. However, it is our belief that the variation is closely linked to a change in end effects and we suspect that elasticity plays here an important role that also requires a future investigation.

7. Conclusions

Measurements of the vortex shedding frequency and formation length were carried out for flow around cylinders with Newtonian and shear-thinning aqueous solutions of methyl hydroxyethyl cellulose (tylose) and carboxymethyl cellulose (CMC). The approach flow was uniform with a free-stream turbulence intensity varying between 3 and 5% at the highest Reynolds numbers. Rheological measurements and the results of hydrodynamic investigations in other complex flows showed the CMC solutions to be elastic and the tylose solutions to be weakly elastic, in both cases with the elastic characteristics increasing with polymer concentration.

This investigation encompassed the transition and the shear-layer transition regimes, with laminar vortex shedding observed with the more concentrated solutions only. One particular definition of Reynolds number (Re^*) was adopted, aimed at the equality of Re_{vs} from Newtonian literature data and from the measurements with 0.4 and 0.3% CMC solutions in all cases for an $L/D = 6$ cylinder. This Reynolds number marks the onset of laminar vortex shedding. The viscosity used in Re^* was calculated at a characteristic shear rate of $U_\infty/(2D)$. The main findings of this work are listed below.

(i) The critical Reynolds numbers marking the onset and end of the various flow regimes and hydrodynamic events were clearly identified and quantified.

(ii) An increase in cylinder aspect ratio and fluid elasticity reduced the various critical Reynolds numbers (Re_{etr}, Re_{lf}, Re_{bbp}). The elastic effect was especially strong with Re_{etr}: for instance Re_{etr} varies from about 667 to 208 for 0.1–0.4% CMC, whereas for the Newtonian fluid it takes the value of 2000.
(iii) The extension of the transition regime was reduced by fluid elasticity and even lead to the suppression of this regime for the 0.6% tylose solution.
(iv) Elasticity was better quantified by the elasticity number Re'/We than by the Weissenberg number. The elasticity number involves the viscosity calculated at a high characteristic shear rate typical of the boundary layer rather than the average value used in Re^*.

Several areas requiring further extensive research were identified: the effect of free-stream turbulence on the flow characteristics of Newtonian and non-Newtonian fluids and the isolated effect of fluid elasticity upon the critical Reynolds numbers by investigating cylinder flow characteristics with Boger fluids.

Acknowledgements

The authors wish to thank JNICT for the financial support through project PBIC/C/CEG/1370/92 and the equipment lent by INEGI and IDMEC. P.M. Coelho also wishes to thank University of Porto for the leave of teaching duties between 1993 and 1996 which made possible a significant portion of this work.

References

[1] V. Strouhal, Ann. Über eine besondere Art der Tonerregung Phys. Chem. (Leipzig) Neue Folge Bd 5 (216) (1878) 10.
[2] K. Hiemenz, Die Grenzschicht an einem in dem gleichförmigen Flüssigkeitsstrom eingetauchten geraden Kreiszylinder, Ph.D. Thesis, University of Göttingen, Germany.
[3] T. von Kármán, Über den Mechanismus dem Widerstands, den ein bewegter Korper in einer Flussigkeit erfahrt, Göttingen Nachr. Math. Phys. Kl. 12 (1912) 509.
[4] B. Cantwell, D. Coles, An experimental study of entrainment and transport in turbulent near wake of a circular cylinder, J. Fluid Mech. 136 (1983) 321–374.
[5] D.P. Telionis, M. Gundappa, T.E. Diller, On the organisation of flow and heat transfer in the near wake of a circular cylinder in steady and pulsed flow, ASME J. Fluids Eng. 114 (1992) 348–355.
[6] C.H.K. Williamson, Vortex dynamics in the cylinder wake, Ann. Rev. Fluid Mech. 28 (1996) 477–539.
[7] J.H. Gerrard, The mechanics of the formation region of vortices behind bluff bodies, J. Fluid Mech. 25 (1966) 401–413.
[8] S.M. Bloor, The transition to turbulence in the wake of a circular cylinder, J. Fluid Mech. 19 (1964) 290–304.
[9] O. Manero, B. Mena, On the slow flow of viscoelastic liquids past a circular cylinder, J. Non-Newtonian Fluid Mech. 9 (1981) 379–387.
[10] P.Y. Huang, J. Feng, Wall effects on the flow of viscoelastic fluids around a circular cylinder, J. Non-Newtonian Fluid mech. 60 (1995) 179–198.
[11] M.J. Shah, E.E. Petersen, A. Acrivos, Heat transfer from a cylinder to a power-law non-Newtonian fluid, AIChE J. 8 (1962) 542–549.
[12] D.F. James, A.J. Acosta, The laminar flow of dilute polymer solutions around circular cylinders, J. Fluid Mech. 42 (1970) 269–288.
[13] D.F. James, O.P. Gupta, Drag on circular cylinders in dilute polymer solutions, Chem. Eng. Prog. Symp. Ser. 67 (111) (1971) 62–73.
[14] T. Sarpkaya, P.G. Rainey, R.E. Kell, Flow of dilute polymer solutions about circular cylinders, J. Fluid Mech. 57 (1973) 177–208.
[15] G.E. Gadd, Effects of long-chain molecule additives in water on vortex streets, Nature 211 (1966) 169–170.
[16] A. White, Drag of spheres in dilute high polymer solutions, Nature 216 (1967) 994–995.

[17] V.N. Kalashnikov, A.M. Kudin, Kármán vortices in the flow of drag-reducing polymer solutions, Nature 225 (1970) 445–446.
[18] H. Usui, T. Shibata, Y. Sano, Kármán vortex behind a circular cylinder in dilute polymer solutions, J. Chem. Eng. Jpn. 13 (1980) 77–79.
[19] O. Cadot, S. Kumar, Experimental characterisation of viscoelastic effects on two- and three-dimensional shear instabilities, J. Fluid Mech. 416 (2000) 151–172.
[20] C. Bergins, M. Nowak, M. Urban, The flow of a dilute cationic surfactant solution past a circular cylinder, Exp. Fluids 30 (2001) 410–417.
[21] J.R. Cressman, Q. Bailey, W.I. Goldburg, Modification of a vortex street by a polymer additive, Phys. Fluids 13 (2001) 867–871.
[22] P.J. Oliveira, Method for time-dependent simulations of viscoelastic flows: vortex shedding behind cylinder, J. Non-Newtonian Fluid Mech. 101 (2001) 113–137.
[23] M. Brede, H. Eckelmann, D. Rockwell, On secondary vortices in the cylinder wake, Phys. Fluids 8 (1996) 2117–2124.
[24] M. Hammache, M. Gharib, An experimental study of the parallel and oblique vortex shedding from circular cylinders, J. Fluid Mech. 232 (1991) 567–590.
[25] C.H.K. Williamson, Defining a universal and continuous Strouhal–Reynolds number relationship for the laminar vortex shedding of a circular cylinder, Phys. Fluids 31 (1988) 2742–2744.
[26] J.H. Gerrard, The three-dimensional structure of the wake of a circular cylinder, J. Fluid Mech. 25 (1966) 143–164.
[27] C.H.K. Williamson, Mode A secondary instability in wake transition, Phys. Fluids 8 (1996) 1680–1682.
[28] H.-Q. Zhang, F. Uwe, B.R. Noack, M. König, H. Eckelmann, On the transition of the cylinder wake, Phys. Fluids 7 (1995) 779–794.
[29] M.F. Unal, D. Rockwell, On vortex formation from a cylinder. Part 1. The initial instability, J. Fluid Mech. 190 (1988) 491–512.
[30] A. Prasad, C.H.K. Williamson, The instability of the shear layer separating from a bluff body, J. Fluid Mech. 333 (1997) 375–402.
[31] M.P. Escudier, I.W. Gouldson, A.S. Pereira, F.T. Pinho, R.J. Poole, On the reproducibility of the rheology of shear-thinning liquids, J. Non-Newtonian Fluid Mech. 97 (2001) 99–124.
[32] G.S. West, C.J. Apelt, The effects of tunnel blockage and aspect ratio on the mean flow past a circular cylinder with Reynolds number between 10^4 and 10^5, J. Fluid Mech. 114 (1982) 361–377.
[33] E.C. Maskell, A theory of blockage effects on bluff bodies and stalled wings in a closed wind tunnel, R&M, No. 3400, 1963.
[34] C. Farell, S. Carrasquel, O. Güven, V.C. Patel, Effect of wind-tunnel on the flow past circular cylinders and cooling tower models, J. Fluids Eng. 99 (1977) 470–479.
[35] D. Gerich, H. Eckelmann, Influence of end plates and free ends on the shedding frequency of circular cylinders, J. Fluid Mech. 122 (1982) 109–121.
[36] R. Stäger, H. Eckelmann, The effect of endplates on the shedding frequency of circular cylinders in the irregular range, Phys. Fluids A 3 (9) (1991) 2116–2121.
[37] C. Norberg, An experimental investigation of the flow around a circular cylinder: influence of aspect ratio, J. Fluid Mech. 258 (1994) 287–316.
[38] M. Stieglmeier, C. Tropea, A miniaturised, mobile laser-Doppler anemometer, Appl. Opt. 111 (1992) 4096–4099.
[39] C. Tropea, 1993 DFLDA Technical Reference Manual, INVENT GmbH, Appendix B.
[40] W.H. Press, S.A. Teukolsky, W.T. Vetterling, B.P. Flannery, Numerical Recipes in Fortran, Cambridge University Press, Cambridge, 1992.
[41] H.W. Coleman, W.G. Steele, Experimentation and Uncertainty Analysis for Engineers, Wiley, New York, 1989.
[42] P.M. Coelho, Flow of non-Newtonian fluids around a cylinder, Ph.D. Thesis, University of Porto, Portugal, 2000 (in Portuguese).
[43] R.B. Bird, R.C. Armstrong, O. Hassager, Dynamics of polymeric liquids, vol. 1, Fluid Mechanics, Wiley, New York, 1987.
[44] P.M. Coelho, F.T. Pinho, Comportamento Reológico de Algumas Soluções Aquosas Diluídas de Polímero, Mecânica Exp. 3 (1998) 51–61.
[45] A.S. Pereira, F.T. Pinho, Turbulent pipe flow characteristics of low molecular weight polymer solutions, J. Non-Newtonian Fluid Mech. 55 (1994) 321–344.
[46] F.T. Pinho, J.H. Whitelaw, Flow of non-Newtonian fluids in a pipe, J. Non-Newtonian Fluid Mech. 34 (1990) 129–144.
[47] G. Astarita, G. Marrucci, Principles of Non-Newtonian Fluid Mechanics, McGraw-Hill, London, 1974.

[48] M.P. Escudier, P.J. Oliveira, F.T. Pinho, Fully developed laminar flow of purely viscous non-Newtonian liquids through annuli, including the effects of eccentricity and inner-cylinder rotation, Int. J. Heat Fluid Flow 23 (2002) 52–73.
[49] A.B. Metzner, J.C. Reed, Flow of non-Newtonian fluids—correlation of the laminar, transition and turbulent flow regions, AIChE J. 1 (1955) 434–440.
[50] J.H. Gerrard, The wakes of cylindrical bluff bodies at low Reynolds number, Phil. Trans. R. Soc. Lond. Ser. A 288 (1978) 351–382.
[51] F.M. White, Viscous Fluid Flow, second ed., McGraw-Hill, New York, 1991.
[52] M. Nishioka, H. Sato, Measurements of velocity distributions in the wake of a circular cylinder at low Reynolds numbers, J. Fluid Mech. 65 (1) (1974) 97–112.
[53] T. Lee, R.A. Budwig, Study of the effect of aspect ratio on vortex shedding behind circular cylinders, Phys. Fluids A 3 (2) (1991) 309–315.
[54] P.M. Coelho, F.T. Pinho, Vortex shedding regimes in cylinder flow of shear-thinning fluids. II. Flow characteristics, J. Non-Newtonian Fluid Mech. 110 (2–3) (2003) 183–199.
[55] R.W. Serth, K.M. Kiser, A solution of the two-dimensional boundary-layer equations for an Ostwald–deWaele fluid, Chem. Eng. Sci. 22 (1967) 945–956.
[56] A.H.P. Skelland, Non-Newtonian Flow and Heat Transfer, Wiley, New York, 1967.
[57] P.M. Coelho, F.T. Pinho, A.R. Rodrigues, The flow of shear-thinning fluids around a cylinder: vortex shedding and drag characteristics, in: Proceedings of the 8th International Symposium on Applications of Laser Techniques of Fluid Mechanics, vol. II, 1996, pp. 35.5.1–35.5.8.
[58] C. Chyu, J.-C. Lin, J. Sheridan, D. Rockwell, Kármán vortex formation from a cylinder: role of phase-locked Kelvin–Helmholz vortices, Phys. Fluids 7 (1995) 2288–2290.
[59] D.A. White, Drag coefficients for spheres in high Reynolds number flow of dilute solutions of high polymers, Nature 212 (1966) 277–278.
[60] A. Acharya, R.A. Mashelkar, J. Ulbrecht, Flow of inelastic and viscoelastic fluids past a sphere. II. Anomalous separation in the viscoelastic fluid flow, Rheol. Acta 15 (1976) 471–478.
[61] J.D. D'Alessio, J.P. Pascal, Steady flow of a power-law fluid past a cylinder, Acta Mech. 22 (1996) 395–405.
[62] J. Azaiez, G.M. Homsy, Linear stability of free shear flow of viscoelastic liquids, J. Fluid Mech. 268 (1994) 37–69.
[63] S. Kumar, G.M. Homsy, Direct numerical simulation of hydrodynamic instabilities in two- and three-dimensional viscoelastic free shear layers, J. Non-Newtonian Fluid Mech. 83 (1999) 249–276.